Precambrian Research 379 (2022) 106786

Contents lists available at ScienceDirect

Precambrian Research

journal homepage: www.elsevier.com/locate/precamres

Paleomagnetism and $^{40}Ar/^{39}Ar$ geochronology of Meso-Neoproterozoic rocks from southwest Norway. Implications for magnetic remanence ages and the paleogeography of Baltica in a Rodinia supercontinent context

Evgeniy V. Kulakov [a,b,*], Trond Slagstad [c], Morgan Ganerød [c], Trond H. Torsvik [a,d]

[a] Centre for Earth Evolution and Dynamics (CEED), University of Oslo, PO Box 1028, Blindern NO-0315, Norway
[b] Northland Pioneer College, 1001 W Deuce of Clubs, Show Low, AZ 85901, United States
[c] Geological Survey of Norway, Trondheim, Norway
[d] School of Geosciences, University of Witwatersrand, Johannesburg 2050, South Africa

A B S T R A C T

Here we present new $^{40}Ar/^{39}Ar$ geochronology, rock magnetic, and paleomagnetic data obtained from rocks from three distinct domains of the Precambrian Sveconorwegian orogen (Southern Norway) that record progressively younger orogenic events from east to west. The first locality is in the Bamble lithotectonic unit and the other two areas are located within the Telemark and Rogaland–Vest Agder sectors in the central and southwestern parts of the Telemark lithotectonic unit, respectively. New and existing geochronology data on metamorphism and cooling, combined with detailed rock magnetic analyses indicate that studied rocks cooled and blocked (acquired) the natural remanent magnetization at ~ 1090 Ma (Bamble Lithotectonic unit), 1000 Ma (Central Telemark), and at around 900 Ma in the westernmost part of the Telemark Lithotectonic Unit. Accordingly, the new paleomagnetic poles for the Bamble (P_{lat} = -6.6°N, P_{long} = 218.4°E, N = 38, A_{95} = 6.1°, K = 15.6), central Telemark (P_{lat} = -17.4° N, P_{long} = 229.8° E, N = 23. A_{95} = 6.5 °, K = 22.6), and western Telemark Lithotetonic Unit (P_{lat} = -46.2° N, P_{long} = 209.4° E, N = 9, A_{95} = 12.0, K = 19.4) were assigned 1090 Ma, 1000 Ma, and 900 Ma ages, respectively. The new Bamble paleomagnetic pole reconstructs Baltica at ~ 1090 Ma with noticeable latitudinal gap from the eastern Laurentian margin and thus does not support classical Baltica-Laurentia configuration within the Rodinia supercontinent. The other two younger poles, when used together with the coeval paleomagnetic data from Laurentia do not support the traditionally envisaged Meso- to Neoproterozoic Baltica-Laurentia relationship either. Overall, the new data do not lend any support to the close connection between the two continents during the proposed Rodinia tenure but instead emphasize the problems with the traditional paleogeographic reconstructions of Rodinia. The new data appear more in line with the geological record within the Sveconorwegian orogen, which indicates that the orogeny developed at or behind active continental margins. While Baltica and Laurentia may have resided at broadly similar latitudes between 1000 and 900 Ma, there is no geologic and paleomagnetic evidence for placing them next to each other.

1. Introduction

The ~ 1140–900 Ma Sveconorwegian orogen (SNO) in SW Baltica is traditionally viewed as a continuation of the Grenville orogen in eastern North America (Laurentia), formed due to collision with a third continental block, often referred to as Amazonia, during the assembly of the Rodinia supercontinent. The Grenville–Sveconorwegian association, which has long been assumed based on temporal similarities and apparent analogies in orogenic style, is common for nearly all, otherwise largely diverse Rodinia models (e.g., Weil et al., 1991; Hoffman et al., 1991; Torsvik 2003; Li et al., 2008; Evans, 2009, 2013). However, the two orogens appear to reflect significantly different tectonic settings, albeit temporarily overlapping. The Grenville orogen is generally inferred to represent a continent–continent collision with its major part characterized by large-scale frontal-thrust ramp tectonics, resulting in the development of a wide orogenic plateau (Culshaw et al., 1997; Rivers, 2012, 2015). The northeastern-most part of the Grenville orogen, usually reconstructed against the SNO in SW Baltica, was, however, only peripherally affected by the main Grenvillian orogenesis and displays contrasting tectonic features such as southeast-trending dextral strike-slip faults of Grenvillian age (Gower et al., 2008). In addition, the Grenvillian metamorphism does not follow the traditionally envisaged east to northeast-trending path into the Atlantic but makes a 90° turn to the southeast. These observations were interpreted as indicating that the SNO may not be a direct continuation of the Grenville orogen (Gower et al., 2008).

In early tectonic models, the SNO was argued to reflect Andean-type accretionary tectonics as the principal process driving orogenesis (e.g., Falkum and Petersen, 1980; Gower, 1985). Since the early 1990 s, the views on the SNO have changed dramatically, so that

* Corresponding author.

https://doi.org/10.1016/j.precamres.2022.106786
Received 21 January 2022; Received in revised form 23 June 2022; Accepted 30 June 2022
Available online 13 July 2022

continent–continent collision became a preferred and largely undisputed model (e.g., Bingen et al., 2008b, Möller et al., 2015, Romer, 1996, Tual et al., 2017). This transformation has mainly been driven by work within the eastern part of the province, where high-pressure metamorphism, large-scale thrusting, and the overall tectonic style superficially resemble those in the Grenville orogen (Gower, 1985; Gower, et al., 1990). More recent work, however, has revived the early views on the SNO (Blereau et al., 2017; Bybee et al., 2014; Slagstad et al., 2013; 2017; 2018b; 2020) and showed that the observed magmatic and metamorphic features across the orogen are difficult to reconcile with both continent–continent collision (e.g. Slagstad et al., 2019) and/or some form of vertical tectonics recently proposed as an alternative model for Sveconorwegian orogenesis (Bingen et al., 2018, 2020; Bingen and Viola, 2018). Instead, the observed features are more compatible with processes expected at or behind active continental margins (Slagstad et al., 2013; Coint, et al., 2015), and interpreted to reflect the reamalgamation of a series of rifted units along the southwestern margin of Fennoscandia (Slagstad et al., 2020). The presence of a subduction system, which operated until at least ~ 940 Ma along the SW margin of Baltica, has recently been confirmed by Corfu (2019). Temporarily overlapping by several tens of million years with the widely adopted period of Baltica–Laurentia–Amazonia conjunction, an active-margin system does not fit spatially nor temporarily into the 'conventional' continent–continent collision models that link the Grenville–Sveconorwegian–Sunsas orogens. Instead, this system underscores the fundamental differences between the orogenic systems and further

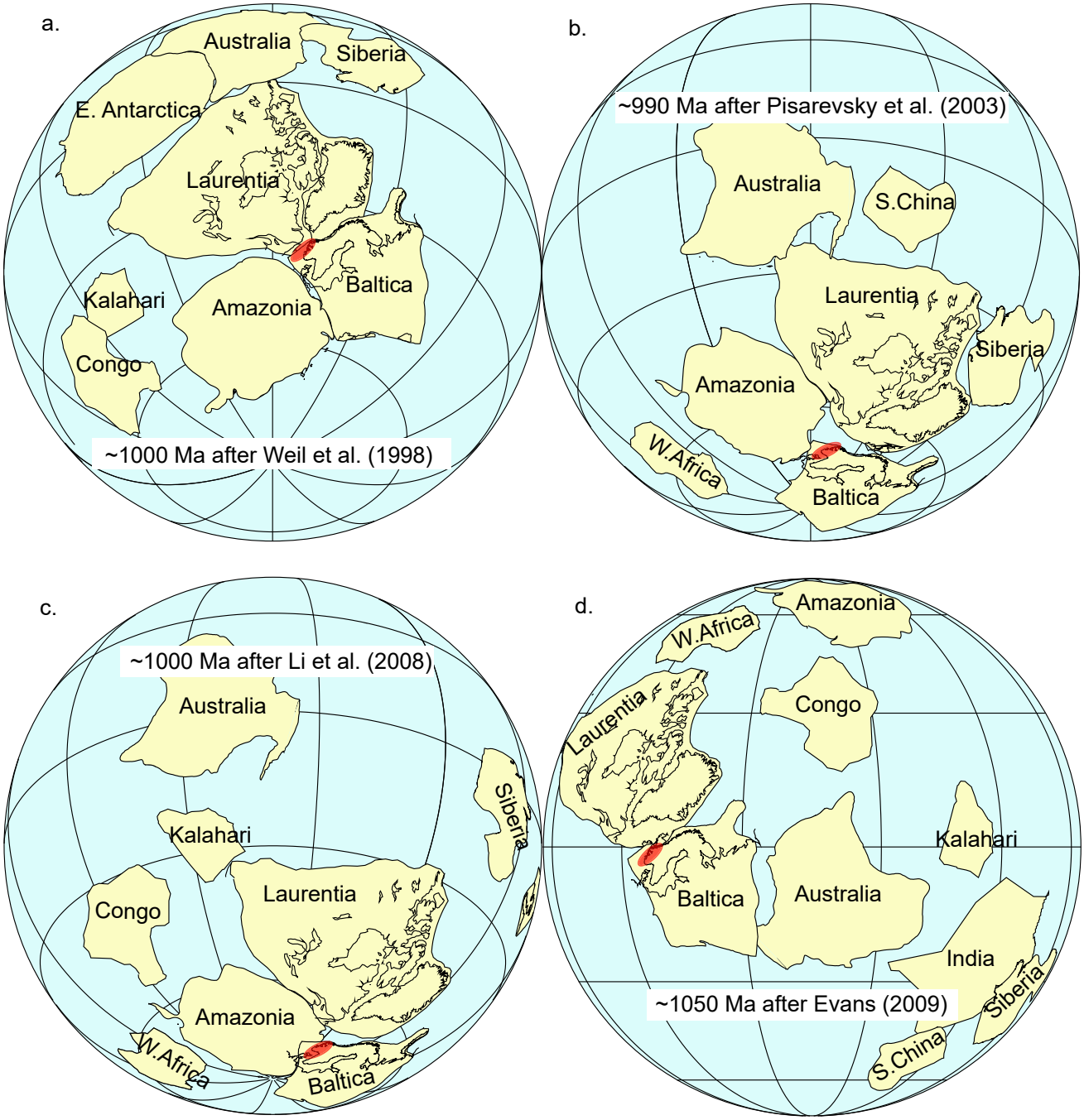

Fig. 1. Different models of the supercontinent Rodinia (see text): **(a)**, after Weil et al. (1998); **(b)**, after Pisarevsky et al. (2003); **(c)**, "consensus" Rodinia of Li et al. (2008), **(d),** Rodinia after Evans (2009). Note the relative positions of Baltica and Laurentia. Shaded in red area is the Sveconorwegian orogeny.

points to a deficiency in the traditional 'triple-junction' model for the three continents. Thus, the position of Baltica within core-Rodinia, the time of final Rodinia assembly, and the overall configuration of the supercontinent must be reconsidered.

Paleomagnetism has been and remains the principal tool in quantitative assessments of past paleolatitudes and orientations of Precambrian cratons. Unfortunately, independent paleomagnetic assessment of the relative position of Baltica with respect to other Rodinia core constituents is hampered by the general scarcity of paleomagnetic data, particularly for the most critical time interval between ~ 1100 and 900 Ma. In addition, most of the available paleomagnetic data for Laurentia and Baltica for the late Mesoproterozoic and early Neoproterozoic have been derived from high-grade metamorphic rocks of the Grenville and Sveconorwegian orogenic belts (e.g., Poorter, 1975; Stearn and Piper, 1984; Brown and McEnroe, 2012) and/or large intrusions (e.g., Brown and McEnroe, 2004, 2015). Complicated cooling histories of these rocks, resulting in ambiguities in constraining ages of magnetic remanence, introduce large uncertainties in paleogeographic models and make deciphering the Precambrian paleogeography extremely challenging. Owing to these challenges and uncertainties, the debate on the evolution of Rodinia, which started over three decades ago, continues (Fig. 1). For example, the "consensus" Rodinia model of Li et al. (2008), in which the supercontinent finally assembled at ~ 1000 Ma (Fig. 1c), was challenged by a rather radical Rodinia model of Evans (2009), where the supercontinent assembled over a prolonged period between ~ 1100 and 750 Ma (Fig. 1d). The latter model, however, has been shown to fail further paleomagnetic assessments (Evans et al., 2010; Evans et al., 2015; Hanson et al., 2011b), particularly with regard to the paleogeographic positions of the São Francisco/Congo and Kalahari cratons. An alternative scenario of Evans (2013) suggests that contrary to the traditional views on the supercontinent, Rodinia may not have existed as a coherent landmass. Such a diversity of Rodinias and overall ambiguities regarding the supercontinent warrant more research on paleomagnetism, geochronology, and metamorphic histories of the Precambrian cratons in order to advance our understanding of Precambrian paleogeography and the evolution of our planet.

In this contribution, we present new $^{40}Ar/^{39}Ar$ geochronology, rock magnetic, and paleomagnetic data obtained from rocks of the Sveconorwegian province from the Bamble and Telemark lithotectonic units of SW Norway, and discuss the age of magnetic remanence acquisition with implications for paleogeography of Baltica during the proposed time of Rodinia assembly.

2. Geology

2.1. A geological overview

The SW margin of Fennoscandia consists of several units, variably referred to as terranes, domains, or sectors (e.g., Bingen et al., 2005; Andersen 2005) that collectively compose the late Mesoproterozoic – early Neoproterozoic Sveconorwegian orogenic belt (Fig. 2a). For descriptive purposes and to avoid confusion with the use of various names for the SNO components, we refer to the main parts of the orogenic belt as lithotectonic units (LUs) (e.g., Slagstad et al., 2020). Smaller-scale subunits, particularly within the Telemark LU, are referred to as sectors, consistent with the nomenclature of Berthelsen (1980) or Bingen et al. (2005). The lithotectonic units were formed and modified during the ~ 1650–1500 Ma Gothian orogeny and reflect ocean-ward growth along a retreating active continental margin (Åhäll and Connelly, 2008; Andersen et al., 2004; Bingen et al., 2005; Petersson et al., 2015b). Further reworked during the SNO, the LUs record a series of magmatic, metamorphic, and deformational events between 1140 and 920 Ma that reflect significant variations and contrasts in style and timing of tectonic events across the orogen (e.g., Falkum and Petersen, 1980; Slagstad et al., 2020). Several medium- to high-pressure metamorphic events with peaks at ~ 1145–1140 Ma, 1050–1025 Ma, and ~ 990 Ma affected the Bamble, Idefjorden, and Eastern Segment LUs, respectively. The central and western parts of the orogen were in a long-lived extensional tectonic regime, characterized by deposition of thick sedimentary sequences of the Telemark supracrustals, until ~ 1110 Ma, outlasting the high-pressure metamorphism in the Bamble LU by approximately 30 Myr. Further west in the Telemark LU, the Rogaland–Vest Agder sector experienced long-lived magmatism, which lasted for about 150 Myr, between 1070 and 920 Ma, coeval with the emplacement of granitic rocks of the Sirdal Magmatic Belt, along with massif-type anorthosites and a layered intrusion of the Rogaland Igneous Complex (Fig. 2). The contrasting magmatic and metamorphic histories of different units across the SNO were emphasized in a number of recent papers (e.g., Slagstad et al., 2017, 2018, 2020) and interpreted to reflect accretionary processes that took place at or behind an active margin. The active-margin tectonic setting along the SW margin of Baltica during the Neoproterozoic was recently reaffirmed by a study of 985–950 Ma metavolcanic and plutonic rocks of the Sognefell Volcanic – Subvolcanic complex, formed in an arc or back-arc settings at the margin of Baltica and the Asgard Sea (Corfu, 2019).

2.2. Study areas and sampling.

In this study, we focus on three distinct domains of the SNO that recorded progressively younger Sveconorwegian orogenic events from east to west. The first locality is in the Bamble LU and the other two areas are located within the Telemark and Rogaland–Vest Agder sectors in the central and southwestern parts of the Telemark LU, respectively. In the following sections, we provide a detailed geologic description of the study areas.

2.2.1. The Bamble lithotectonic unit.

The Bamble LU is an approximately 30 km-wide high-grade metamorphic unit, located along the southern coast of Norway (Fig. 2a, b). It is bound by the Permian Oslo rift to the northeast and strikes southwest to the city of Kristiansand. Lithologically, it contains variably migmatitic granitic orthogneisses with protolith ages between 1600 and 1500 Ma and major- and trace-element compositions suggestive of formation in a continental magmatic arc (Andersen et al., 2004). Quartz-rich and metapelitic metasedimentary rocks reflect shallow-water turbiditic deposits with maximum depositional ages ranging between ~ 1500 and 1400 Ma (de Haas et al., 1999; Slagstad et al., 2020). The Bamble orthogneisses and metasediments were later intruded by mafic and felsic magmas with igneous crystallization ages between 1235 and 1135 Ma and further reworked during the SNO. The Bamble LU also hosts two post-tectonic (~980 and 920 Ma) undeformed granitic plutons, which effectively stitch the Bamble and Telemark LUs and mark the lower age limit for the cessation of Sveconorwegian orogenesis within the Bamble LU. The Bamble rocks exhibit a transition from granulite- to amphibolite-facies metamorphism. Granulite-facies metamorphism peaked between ~ 1145 and 1125 Ma (Knudsen et al., 1997; Knudsen and Andersen, 1999; Cosca et al., 1998; Bingen et al., 2008), followed by a protracted period of decreasing P-T conditions and attendant regional cooling of the Bamble LU to temperatures below ~ 550 °C between ~ 1110 and 1080 Ma (Cosca et al., 1998; Slagstad et al., 2020) Ma. The rapid cooling of the Bamble LU, with estimated cooling rates likely exceeding 10–12°/Myr (Slagstad et al., 2020), was interpreted to reflect its thrusting onto adjacent Telemark LU (Slagstad et al., 2020). A well-documented episode of metasomatism affected rocks within the Bamble LU and resulted in widespread scapolitisation, albitization, and development of hydrothermal apatite, rutile, and Fe deposits (Engvik and Austrheim, 2010; Engvik et al., 2018). U–Pb dating of rutile from scapolite metagabbro and albitite yielded ages of 1090–1084 Ma. Although questionable, based on the relatively low U–Pb closure temperatures in rutile (~450 °C), these ages were interpreted as indicative of timing of regional cooling rather than the timing of metasomatism, which must have occurred at significantly higher temperatures (Engvik

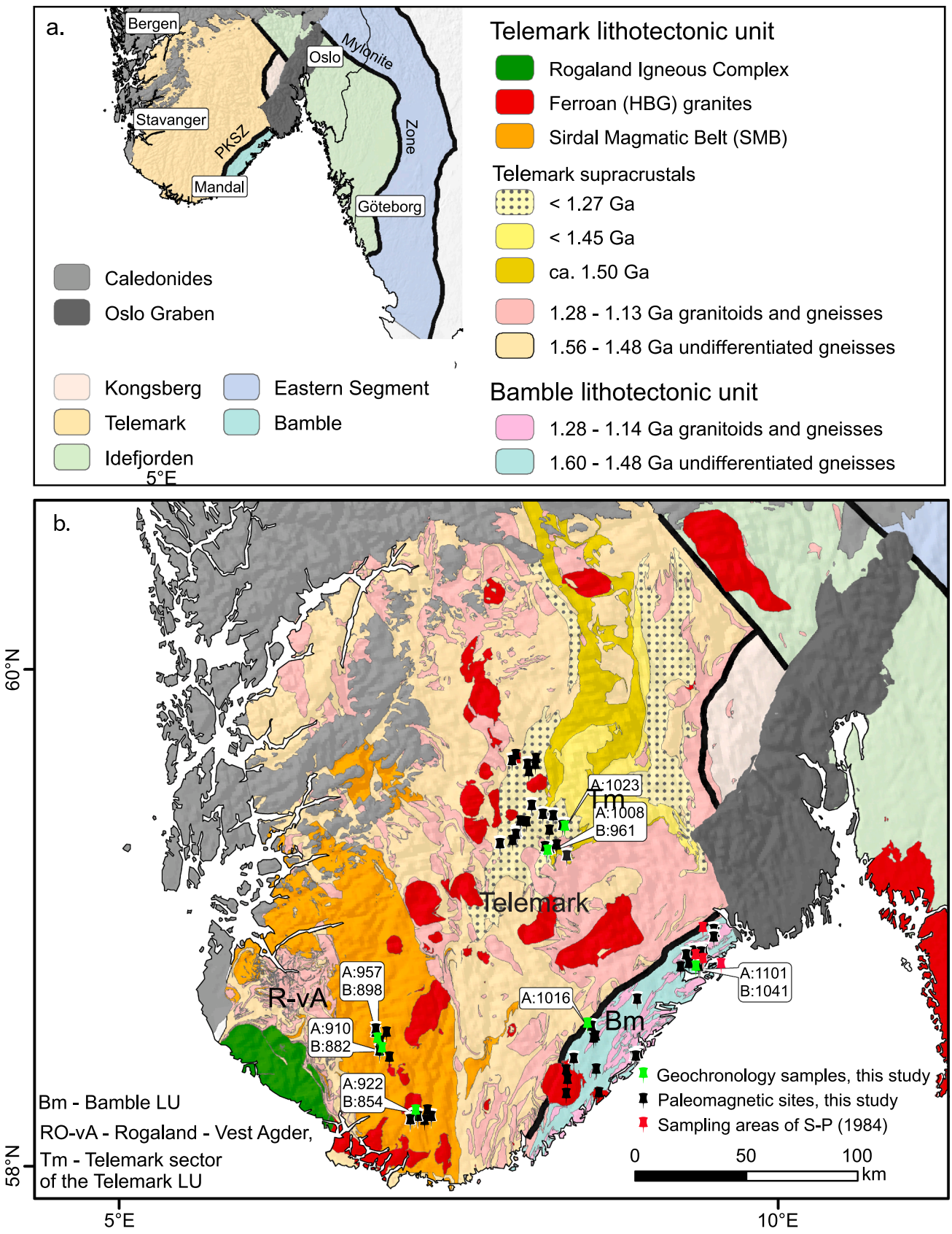

Fig. 2. (a) Map of the southwestern part of Baltica showing lithotectonic units (LUs) of the Sveconorwegian orogeny (SNO). **(b)** Sampling areas within the Bamble LU and Telemark and Rogaland–Vest Agder sectors of the Telemark LU. Black (green) stars show our paleomagnetic (Ar-Ar geochronology) sampling locations. Red stars show paleomagnetic sampling areas of Stearn and Piper (1984), see text. Numbers in boxes indicate $^{40}Ar/^{39}Ar$ ages reported here (see text). "A" and "B" in the boxes indicate amphibole (hornblende) and biotite ages, respectively.

et al., 2011).

2.2.2. Central part of the Telemark lithotectonic unit. The Telemark sector

The Telemark LU (Fig. 2b), separated from the Bamble LU by the Porsgrunn–Kristiansand shear zone (PKSZ), constitutes a major part of the SNO. A predominant extensional tectonic regime (e.g., Slagstad et al., 2020), lasting until at least 1110 Ma within the Telemark sector, was accompanied by deposition of a geographically widespread, thick sedimentary/volcanic sequence known as the Telemark supracrustals. This sequence was later affected by mainly greenschist- and locally, immediately near the PKSZ, amphibolite-facies metamorphism. The lowermost part of the Telemark supracrustals consists of ~ 1510–1500 Ma bimodal volcanics of the Rjukan Group. It is overlain by quartzites of the Vindeggen Group, which, in turn, are unconformably overlain by the ~ 1155–1145 Ma bimodal volcanic and sedimentary rocks of the Bandak group (Laajoki et al., 2002). The < 1120 Ma sedimentary rocks of the Eidsborg Formation, Heiddal Group, and the Kalhvold Formation make up the uppermost sequence of the Telemark supracrustals. The Telemark supracrustals experienced at least two major deformation events. The first ~>1155 Ma phase resulted in deformation of the Rjukan and Vindeggen Groups, whereas the second phase that occurred after 1145 Ma, deformed the overlying metavolcanic and sedimentary rocks for the first time and rocks of the Rjukan and Vindeggen groups for the second time (Laajoki et al., 2002). Deformation within the area resulted in moderate – to steep tilting of the supracrustals, which now dip in varying directions, at angles that range between 30 and 85°, forming multiple syn- and antiformal structures.

2.2.3. Southwestern part of the Telemark lithotectonic unit. The Rogaland–Vest Agder sector and the Sirdal Magmatic Belt

The Rogaland–Vest Agder sector in the southwesternmost part of the Telemark LU (Fig. 2b) is traditionally described as a high-grade gneissic terrain that underwent regional high- to ultrahigh-temperature metamorphism between 1030 and 970 Ma, with increasing metamorphic grade towards the western part where the Rogaland Igneous Complex (RIC) intruded at ~ 930 Ma (e.g., Bingen et al., 2008b). More recent studies, however, have shown that the high-grade metamorphism was essentially confined to the SW part and temporarily overlaps with the intrusion of ~ 1070–950 Ma granites, anorthosites, and mafic magmatic rocks (Coint et al., 2015; Bybee et al., 2014). Geological mapping indicates that a major part of the Rogaland–Vest Agder sector is made up of undeformed granitic rocks of the Sirdal Magmatic Belt (SMB), which intruded into already metamorphosed crust (Coint et al., 2015) and largely lack metamorphic overprinting. Petrography and geochronology of the SMB rocks suggest prolonged emplacement of the SMB between ~ 1070 and 1020 Ma. The SMB contains north–south-oriented zones rich in xenoliths of variable composition that may represent the former host rocks to the intrusions. The xenolith-rich zones, therefore, may reflect contacts between different intrusions or plutons. In the study area, in the central and southern parts of the SMB, the ~ 1035 Ma granites host xenoliths of granitic gneiss, foliated granite, migmatitic gray gneiss, and amphibolite (Coint et al., 2015).

2.2.4. Sampling

A total of 343 oriented samples were collected from 35 sites of gabbros and amphibolites, and 9 sites from post-tectonic granites of the Bamble LU. Over 260 samples from 33 sites of the Telemark volcanics of the Bandak Group, and 142 samples from 18 individual amphibolitic xenoliths within the Sirdal Magmatic Belt in the Rogaland–Vest Agder sector (Fig. 2b) of the Telemark LU. Amphibolitic xenoliths were given preference as paleomagnetic targets over SMB granites because of their greater potential to record and preserve a paleomagnetic signal compared to granites or gneisses. The samples were collected using a standard paleomagnetic gasoline-powered drill and oriented with magnetic and sun compass readings. Block samples for $^{40}Ar/^{39}Ar$ geochronology study were taken from the same outcrops.

3. Methods

3.1. $^{40}Ar/^{39}Ar$ geochronology

Six samples, representing rocks from the central and western Telemark LU, were analyzed for their $^{40}Ar/^{39}Ar$ isotopic composition (see Supplementary material for details, Supplementary Data, Table S1). $^{40}Ar/^{39}Ar$ isotope analyses were performed at the geochronology laboratory of the Geological Survey of Norway (Trondheim). We calculated irradiation parameters (J-values) relative to an age of 1080.4 ± 1.1 Ma for the PP2 hornblende flux monitor (Renne et al., 2010). Age plateaus were defined according to the following requirements: at least three consecutive spectrum steps, overlapping at the 95% confidence level (1.96σ) and comprising at least 50% of total ^{39}Ar with a mean square of weighted deviates (MSWD) less than the two-tailed student T critical value (for n – 1 degrees of freedom, where n is the number of accepted consecutive spectrum steps). The radiometric ages were calculated as means of accepted consecutive steps, weighted by the inverse of the analytical variance.

3.2. Rock and paleomagnetism

Rock magnetic and paleomagnetic analyses were carried out in the Ivar Giæver Geomagnetic Laboratory at the University of Oslo. A minimum of two representative samples from each site was examined for their rock-magnetic properties. Thermomagnetic (low-field magnetic susceptibility versus temperature) measurements were made using an AGICO MFK1–FA magnetic susceptibility meter (kappabridge) equipped with a high-temperature furnace. The thermomagnetic κ(T) curves were measured upon cycling from room temperature to 700 °C and back to room temperature in an inert atmosphere (argon). Magnetic hysteresis parameters (coercivity, H_c; coercivity of remanence, H_{cr}; saturation remanence and saturation magnetic moments, M_{rs}, M_s;) and first-order reversal curves (FORCs) were measured using a Lake Shore PMC MicroMag 3900 Vibrating Sample Magnetometer (VSM).

We also examined the opaque mineralogy of our samples using a Hitachi SU5000 field-emission scanning electron microscope (FE–SEM, Schottky FEG), equipped with a low-vacuum mode and in-lens secondary electron (SE) and energy dispersive spectra (EDS) detectors. The SEM analyses were conducted on at least one representative sample from each lithology (except for the post-tectonic granites) from all three LUs. Backscattered electron imaging was used to identify oxide grains. The composition of the oxide grains was determined using energy dispersive spectrometry. The spectra were measured at 8 to 15 keV accelerating voltage.

Natural remanent magnetization (NRM) of all samples was measured using an automated AGICO JR–6A spinner magnetometer or a WSGI Model 755 superconducting rock magnetometer (SRM), both hosted in low-magnetic field cages. Paleomagnetic samples were stepwise thermally and/or alternating-field (AF) demagnetized using an MMTD80A automatic, microprocessor-controlled thermal demagnetizer and the SRM in-line AF demagnetization unit, respectively. Progressive demagnetization (typically 15–20 steps, depending on magnetic mineralogy) was carried out until the NRM intensity of the specimens became erratic and unstable or decreased below the instrumental sensitivity. NRM components were isolated using principal-component analysis (Kirschvink, 1980). In a few cases of overlapping unblocking temperatures and coercivities, the great remagnetization circles method (Halls, 1976) was used to determine directions of magnetic remanence. Site-mean and group mean (a mean paleomagnetic direction calculated from a group of site means, combined by the study area and magnetization polarity) paleomagnetic directions were calculated using Fisher statistics (Fisher, 1953). A site-mean direction was accepted if calculated from at least three individual samples' paleomagnetic directions and the radius of the associated 95% confidence circle (α_{95}) not exceeding 15°.

4. Results

4.1. $^{40}Ar/^{39}Ar$ geochronology

4.1.1. The Bamble lithotectonic unit

$^{40}Ar/^{39}Ar$ geochronology data from the Bamble LU have been reported in Slagstad et al. (2020). Sample BM18, from gabbro exposed near the town of Kragerø in the NE part of the Bamble LU, yielded a hornblende age of 1101 ± 4 Ma and biotite age of 1041 ± 1 (Slagstad et al., 2020; Fig. 3a, b, Table 1), which agrees well with previously reported $^{40}Ar/^{39}Ar$ cooling ages for the Bamble LU (e.g., Cosca and O'Nions, 1994). In addition, an amphibolite sampled nearthe contact with the PKSZ, separating the Bamble and underlying Telemark LUs, yielded hornblende and biotite ages of 1016 ± 3 (Fig. 3c) and 920 ± 2 Ma

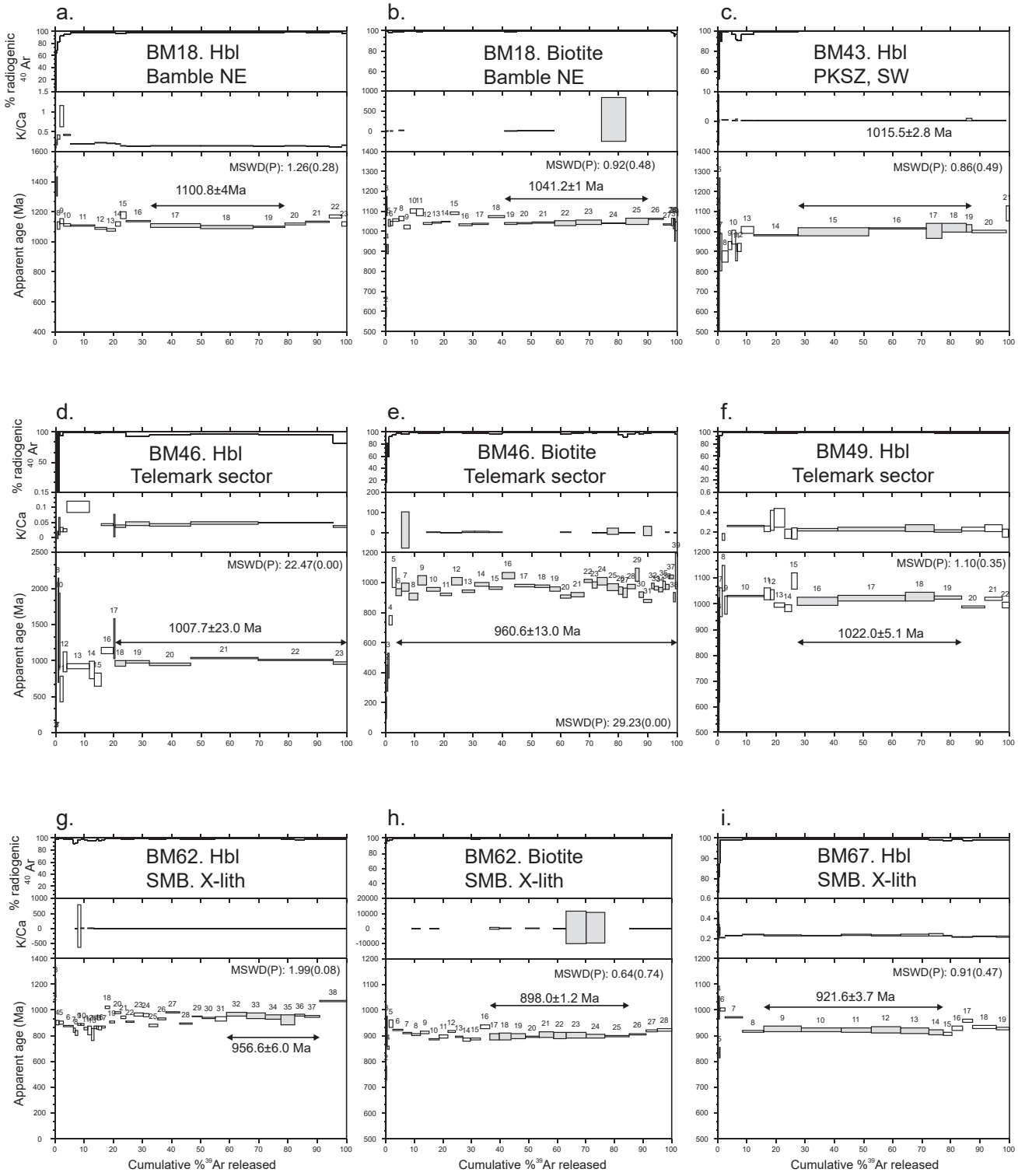

Fig. 3. The results of $^{40}Ar/^{39}Ar$ incremental heating experiments (degassing spectra) on hornblende and biotite crystals. (a-c) from Bamble samples, (d-f) from Telemark volcanics, and **(g-i)** from mafic xenoliths from the Sirdal Magmatic belt. Data from the Bamble lithotectonic unit have been previously reported in Slagstad et al. (2020). Analytical errors are given at 2σ level.

Table 1
$^{40}Ar/^{39}Ar$ geochronology of studied samples. * - data previously reported in Slagstad et al. (2020). Analytical errors are given at 2σ level. Lat and Long indicate geographic coordinates of the sampling sites. Steps (n) indicate consecutive measurement steps (total number of measurement steps) used to calculate plateau ages (see Supplementary data table S1). MSWD – means square of weighted deviates of calculated plateau ages.

Sample	Material	Lat (°N)	Long (°E)	Steps (n)	%^{39}Ar	Age ± 2 s (Ma)	MSWD (P)
BM18*	Amphibole	58.887	9.421	17–19(3)	46.08	1100.8 ± 4.3	1.26(0.28)
BM18*	Biotite	58.887	9.421	19–25(7)	49.32	1041.2 ± 1.1	0.92(0.48)
BM43*	Amphibole	58.640	8.574	15–19(5)	59.75	1015.5 ± 2.8	0.86(0.49)
BM43*	Biotite	58.640	8.574	35–37(3)	20.94	919.8 ± 2.0	0.16(0.85)
BM46	Amphibole	59.356	8.238	18–23(6)	79.5	1007.7 ± 22.8	22.47(0.00)
BM46	Biotite	59.356	8.238	6–39(34)	96.57	960.6 ± 13.0	29.23(0.00)
BM49	Amphibole	59.451	8.337	16–19(4)	56.41	1022.0 ± 5.2	1.10(0.35)
BM62	Amphibole	58.613	6.903	32–37(6)	31.9	956.6 ± 6.1	1.99(0.08)
BM62	Biotite	58.613	6.903	17–25(9)	48.76	898.0 ± 1.2	0.64(0.74)
BM64	Amphibole	58.540	6.941	8–11(4)	49.41	909.5 ± 5.5	1.62(0.18)
BM64	Biotite	58.540	6.941	23–30(8)	43.9	882.1 ± 1.7	0.91(0.50)
BM67	Amphibole	58.270	7.230	9–14(6)	61.72	921.6 ± 3.9	0.91(0.47)

(Table 1), respectively. For further details on metamorphic, crystallization, and cooling ages for the Bamble LU, we refer readers to plentiful literature (Bingen et al, 2008b; Cosca and O'Nions, 1994; Engvik et al., 2011, 2017; de Haas et al., 2002; Slagstad et al., 2020).

4.1.2. Central part of the Telemark lithotectonic unit. The Telemark sector

$^{40}Ar/^{39}Ar$ isotope analysis was conducted on two samples collected from the Bandak group. Sample BM46 yielded an age of 1008 ± 22 Ma measured from a hornblende crystal. A biotite age from the same sample was measured at 961 ± 13 Ma (Fig. 3d, e; Table 1). The other sample (BM49) yielded a more precise, yet statistically similar, hornblende age of 1023 ± 5 Ma (Fig. 3f, Table 1).

4.1.3. Southwestern part of the Telemark lithotectonic unit. Mafic xenoliths within granites of the Sirdal Magmatic Belt

Three samples from mafic xenoliths within the Sirdal Magmatic Belt (SMB) were analyzed. The hornblende ages range between 957 ± 6 and 910 ± 5 Ma (Fig. 3g, h; Table 1). Biotite crystals extracted from the same samples yielded ages between 898 ± 1 and 854 ± 15 Ma (Table 1; Fig. 3i).

4.2. Rock magnetism and scanning electron microscopy

4.2.1. The Bamble lithotectonic unit

Samples from gabbros and amphibolites of the Bamble LU reveal variable rock magnetic characteristics. Temperature dependences of low-field magnetic susceptibility, κ(T), yielded several types of thermomagnetic curves that indicate rather complex magnetic mineralogy in the studied rocks (see Supplementary information for details). The majority of measured κ(T) curves reveal the presence of a magnetic phase with Curie temperature in a range between ~ 580–590 °C, typical for magnetite (Fig. 4a, b, Supplementary figure S1). Some samples showed an inflection on the heating κ(T) cycle at ~ 320 °C indicating another magnetic phase, which we interpret as monoclinic pyrrhotite (Fig. 4b). In some samples, pyrrhotite appears as the main ferromagnetic phase, while in others minor amounts of the Fe-sulfide co-existed with Fe–Ti oxides (Fig. 4b, c). In addition, samples from many sites of gabbros and amphibolites yielded highly irreversible low-field magnetic susceptibility dependences (Supplementary Figure S1b). These κ(T) curves indicate the presence of two ferromagnetic phases with Curie temperatures of ~ 480–500 °C and 580 °C, suggestive of titanomagnetite and magnetite as the main magnetic minerals. Both temperature peaks become more pronounced upon cooling. We interpret this observation as due to the reduction of partly oxidized magnetic minerals during heating and cooling in an inert atmosphere.

Magnetic mineralogy of the post-tectonic granites is characterized by a single magnetic phase with Curie temperature close to that of magnetite. The thermomagnetic curves measured from granitic samples always displayed some degree of irreversibility with an attendant 10–20% increase in magnetic susceptibility upon cooling (Supplementary Figure S1c).

The majority of measured hysteresis loops had regular shapes, which indicates the presence of a single low- to intermediate-coercivity magnetic phase (Fig. 4d, e). Some samples, however, yielded loops typical for mixtures of magnetic phases with different coercivities (Fig. 4f, Supplementary Figure S 2a). The M_{rs}/M_s and H_{cr}/H_c ratios suggest pseudo-single domain (PSD) magnetic carriers in most of the Bamble samples (Fig. 4g) (Day et al., 1977). Samples in single-domain (SD) state were also detected. First-order reversal curve (FORC) diagrams support the predominant PSD–SD magnetic domain state of the Bamble samples (Fig. 4h and Supplementary Figure S3 a, b).

Hysteresis properties of samples from the two post-tectonic granites indicate a single magnetic phase with low coercivity and M_{rs}/M_s and H_{cr}/H_c ratios typical for multidomain (MD) magnetic grains (Supplementary Figure S2b).

Backscattered electron imaging was used to identify oxide grains that vary in size from over a hundred microns to<10 μm (see Supplementary information for details, Supplementary figure S4 a). Many grains contain one or several subordinate sets of trellis-type lamellae (Haggerty, 1991) (Supplementary figure S4a), indicative of the high-temperature (deuteric) oxidation stage C3 (abundant ilmenite lamellae; equilibrium two-phase intergrowths) of Wilson and Watkins (1967) and Haggerty (1991).

4.2.2. Central part of the Telemark lithotectonic unit. The Telemark sector

Samples from the Telemark sector Bandak group volcanics also display considerable variability in thermomagnetic characteristics (supplementary information). The κ(T) dependences were typically irreversible with varying degrees of irreversibility (Fig. 5a, b). Most of the measured κ(T) indicate the presence of a high-temperature magnetic phase, interpreted as hematite. Some samples, however, exhibited reversible susceptibility–temperature dependences with Curie temperatures of 580–590 °C, suggesting magnetite as the principal magnetic carrier (Fig. 5c). This thermomagnetic behavior was the least common for the Telemark rocks and was observed in samples from two sites only.

The majority of samples yielded hysteresis loops that indicate single-domain to small pseudo-single domain magnetic minerals (Fig. 5d–f, Supplementary Figure S2d–f). Relatively high overall coercivities, typical to most of the Telemark basalt samples, suggest the presence of hematite as the main magnetic phase. The FORC diagrams (Fig. 5h) are characterized by a wide horizontal ridge, typical to SD hematite (Roberts et al., 2000; Roberts et al., 2014), further supporting our interpretation that although magnetite is present in many samples, hematite is the main magnetic phase. Samples that yielded bulk PSD magnetic hysteresis characteristics contain a mixture of two magnetic phases: an MD to PSD low- to intermediate-coercivity phase and an SD, high-coercivity phase, as illustrated by FORC diagrams (Supplementary

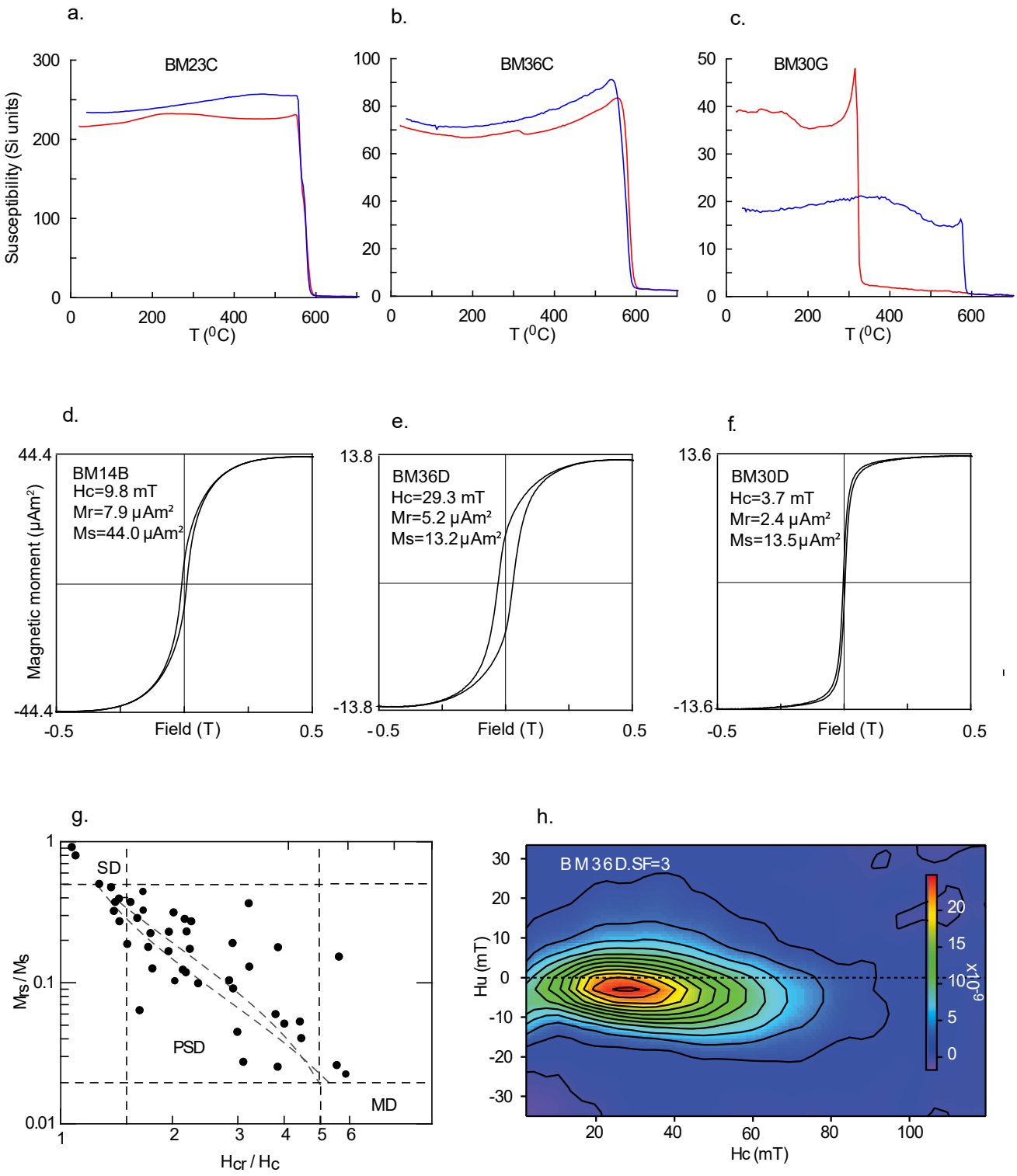

Fig. 4. Rock magnetic properties of Bamble rocks. (a-c): Typical dependence of low-field magnetic susceptibility (κ) versus temperature showing heating (red curves) and cooling (blue curves); **(d-f)**: Typical magnetic hysteresis loops after paramagnetic slope correction; **(g),** Day plot (Day et al., 1977). Abbreviations are the following: SD, single domain; PSD, pseudo-single domain; MD, multidomain; Mrs and; Ms are saturation remanent and saturation magnetic moments, respectively; Hc, coercivity field; Hcr, the coercivity of remanence. Gray dashed lines show SD-MD mixture models from Dunlop (2002); (h), First-order reversal curve (FORC) diagram. The bar legends next to the FORC diagrams show the density of the FORC distribution. SF-indicates the smoothing factor used during the FORC processing. FORC data were analyzed using the FORCinel software (Harrison and Feinberg, 2008). SF – smoothing factor.

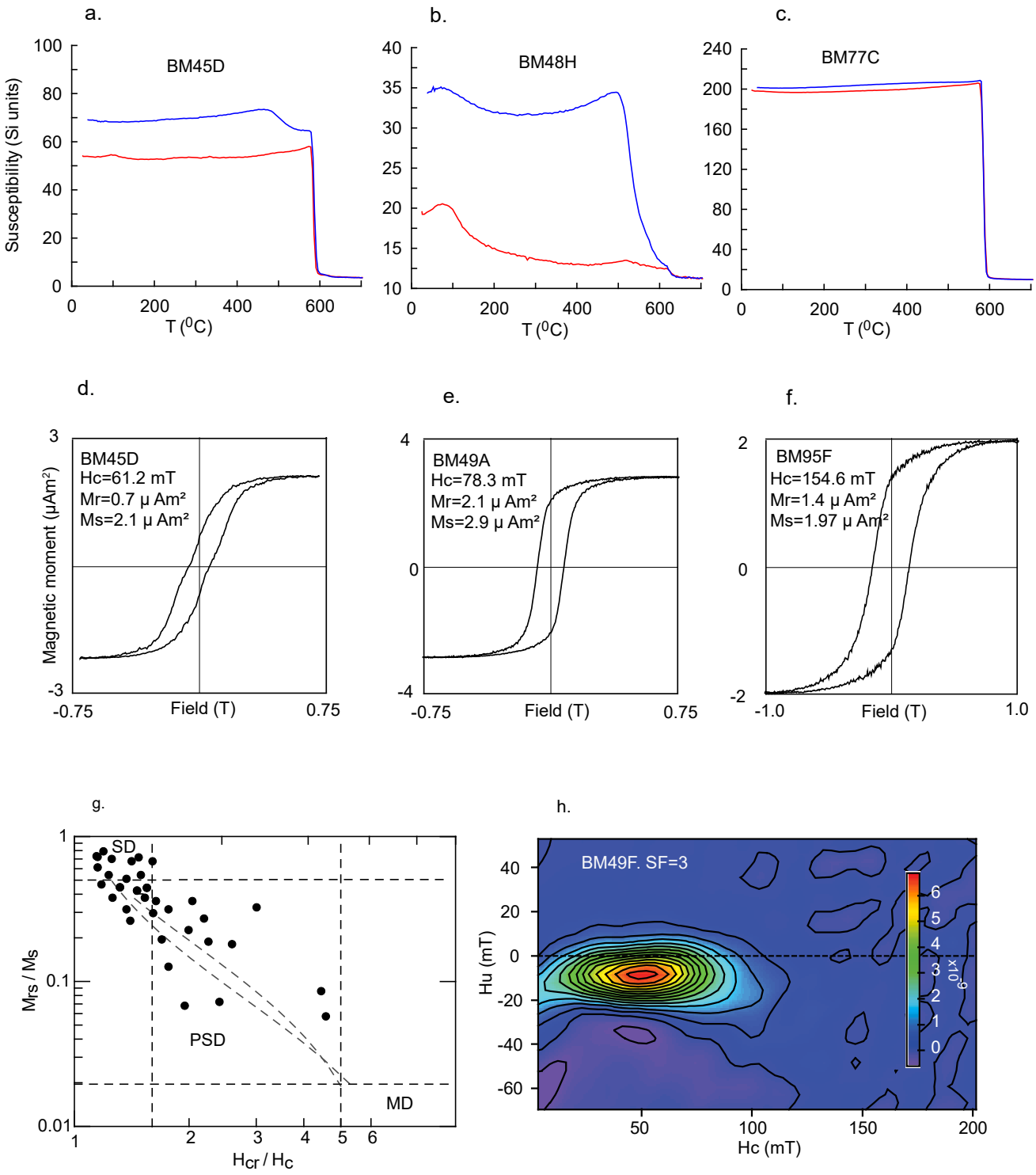

Fig. 5. Rock magnetic properties of central Telemark volcanics. (a-c): Typical dependence of low-field magnetic susceptibility (κ) versus temperature showing heating (red curves) and cooling (blue curves); **(d-f)**: Typical magnetic hysteresis loops after paramagnetic slope correction; **(g),** Day plot (Day et al., 1977); (h), First-order reversal curve (FORC) diagram. Abbreviations and other details are the same as in Fig. 3.

Figure S3d).

Scanning electron microscopy of the Telemark volcanics indicates that the studied samples contain grains of Fe–Ti oxides ranging in size between 10 and 80 μm. Observed grains have well-defined high-temperature oxyexsolution textures with a set of parallel lamellae of ilmenite (Supplementary material figure S4e, g), exsolved within Fe–Ti oxides, which composition is consistent with that of hematite (Supplementary material figure S4f).

Overall, the results of our rock magnetic and microscopy study indicate that single-domain hemoilmenites, characterized by almost pure ilmenite lamellae within the Fe-oxide (hematite) grains are the principal magnetic minerals in Telemark volcanics that carry natural remanent magnetization, probably of chemical or thermochemical origin (Brown and McEnroe, 2012).

4.2.3. Southwestern part of the Telemark lithotectonic unit. Mafic xenoliths within granites of the Sirdal Magmatic Belt

The majority of measured low field magnetic susceptibility versus temperature dependences yielded nearly reversible k(T) curves with characteristic Curie temperatures near that of magnetite (Fig. 6a–c, Supplementary Figure S1g–I, Supplementary information for details). Magnetic hysteresis parameters of mafic xenolith samples suggest PSD to MD magnetic grains in most of the studied samples (Fig. 6d–g). The hysteresis loops suggest the presence of a single magnetic phase with low to intermediate coercivity. A few samples, however, yielded "goose-neck" hysteresis loops, typical for samples with mixtures of magnetic grains with varying coercivities (Fig. 6f). Most of the measured FORC diagrams have a wide vertical spread, and indicate generally low coercivities consistent with the large PSD to MD range of magnetic grains (Fig. 6h, Supplementary Figure S3e). FORC diagrams, measured from the samples that yielded "goose-neck" hysteresis loops, further corroborate our interpretation of the presence of mixtures of magnetic phases with different coercivities (Supplementary information, Supplementary Figure S3f).

Magnetic minerals in mafic xenoliths samples are typically large and vary in size between 100 and 300 μm and have oxide texture consistent with the high-temperature oxidation stage-2 of titanomagnetites (Haggerty, 1991).

4.3. Paleomagnetism

Most of the measured samples yielded a two-component natural remanent magnetization (NRM). For convenience, we refer to low-temperature/coercivity non-characteristic and characteristic high-temperature/coercivity NRM components as secondary and primary characteristic NRM (ChRM), respectively. However, bear in mind that the 'primary' ChRM likely corresponds to a 'new' primary magnetization acquired during the post-peak-metamorphism cooling of the studied rocks. Conversly, 'secondary' NRM components represent younger viscous or thermoviscous NRM overprints.

4.3.1. The Bamble lithotectonic unit

A low-temperature/coercivity NRM component with variable directions was typically removed by demagnetization temperatures in the range between 100 and 300 °C or 5–10 mT alternating field (Fig. 7a, b). The characteristic remanence component (ChRM), identified by straight linear decay to the origin on the vector endpoint diagrams, was demagnetized to<5–10% or below the instrumental sensitivity by 575–585 °C or by AF treatment of 90–100 mT. Some samples displayed a somewhat complex demagnetization behavior. Partly overlapping spectra of unblocking temperatures (but distinct coercivity spectra) of nearly antipodal NRM components resulted in demagnetization trajectories along the arcs of great circles upon thermal demagnetization, followed by straight linear high-temperature/coercivity ChRM segments with clear origin-ward trends on the vector end-point diagrams (Fig. 7 c). The direction of the low-temperature secondary component defined by the great circle intersection technique (Halls, 1976) was nearly antipodal to that of the higher temperature/coercivity ChRM component, suggesting cooling of these rocks through a geomagnetic reversal.

Paleomagnetic data from most sites (N = 20) met our basic statistical acceptance criteria (Table 2). The majority of the site means (N = 11) have NW–NNW directions with negative intermediate inclinations. Four site means have nearly antipodal directions (Table 2, Fig. 7g). Samples from two sites yielded mean paleomagnetic directions similar to the present-day magnetic field. Paleomagnetic data from these sites were excluded from the further calculations. In addition, samples from five sites gave mean SSW paleomagnetic directions with relatively shallow negative inclinations similar to those reported by Stearn and Piper (1984). Fully consistent with the previous study, these NRM components were obtained exclusively from samples with low-coercivity (LC) magnetic minerals. These LC NRM components were completely demagnetized by alternating fields no stronger than 20–30 mT. The authors of the previous study did not make any inferences about the temporal relationship between the SSW LC and more common and more stable NNW directions. We argue that the LC components are likely a younger Permian NRM overprint related to the thermal activity during the Oslo rift development. The SSW LC component and associated virtual geomagnetic pole positions are similar to those, obtained from rocks associated with the Permian Oslo rift (e.g., Torsvik et al., 1998; van Everdigen, 1960). Similar SSW remanence components, isolated from the Precambrian Moelv tillite (Meert, 2014a) and sedimentary rocks of the Fen complex (Dominguez et al., 2011) were also interpreted as due to tectono-thermal events associated with magmatic activity in the Oslo Rift (Meert, 2014a). In addition, the LC remanence has been observed in the samples of a dike that cuts an older gabbroic intrusion of the Bamble LU (site 152 of Stearn and Piper, 1984) and relates to the late Paleozoic volcanic activity. Interestingly, the LC NRM component was observed exclusively in samples closest to the Oslo rift, the north-eastern part of the Bamble LU (Stearn and Piper, 1984; this study). This further supports our interpretation of a Permian age for the LC NRM component. Samples from the 18 rejected sites, including nine sites from the post-tectonic Grimstad and Herefoss granites, yielded chaotic demagnetization trajectories (Fig. 7e, f).

The 15 accepted site-means were combined with the 23 previously published site-mean paleomagnetic directions for the Bamble LU (Stearn and Piper, 1984), selected using the same set of acceptance criteria and excluding 13 SSW shallow and intermediate-inclination normal-polarity site means that reflect younger Permian NRM overprints. The combined set of paleomagnetic site-mean directions contains 31 NNW normal polarity (negative inclination) and seven SSE reversed polarity (positive inclination) site means (Table 2, Fig. 7g). Here we refer to the paleomagnetic directions with negative inclinations as normal-polarity directions assuming that Baltica was located in the southern hemisphere. The mean normal paleomagnetic direction (D = 327.9°, I = -50.7°, α_{95} = 5.7°, k = 21.3, N = 31) marginally passes the reversal test (McFadden and McElhinny, 1990) against the opposite polarity group mean direction (D = 131.7°, I = 51.6°, α_{95} = 13.3°, k = 21.6, N = 7) in classification "*C*". The associated angle between the mean paleomagnetic directions γ = 10.2° and the critical angle γ_c = 13.2°. The calculated mean virtual geomagnetic poles (VGP), corresponding to the sets of normal and reversed paleomagnetic directions, are located at: P_{lat}= − 5.8°N, P_{long} = 216.3°E (A_{95} = 6.8°, K = 15.5, N = 31) and P_{lat} = -10.2°N, P_{long} = 227.4°E (A_{95} = 14.4°, K = 18.4, N = 7), respectively. A paleomagnetic pole (Table 2), calculated from all 38 VGPs is located at: P_{lat} = -6.6°N, P_{long} = 218.4°E (A_{95} = 6.1°, K = 15.6). The new pole merits a 4-point score (5 if structural coherence with the host craton is considered) on the updated paleomagnetic reliability scale (Meert et al., 2020).

4.3.2. Central part of the Telemark lithotectonic unit. The Telemark sector

The secondary, often noisy NRM component in the Telemark samples was usually removed by heating to relatively high temperatures between 400 and 500 °C (Fig. 8a–f). The direction of this component was typically opposite to that of the characteristic NRM. Alternating field demagnetization in fields up to 150–160 mT did not result in full demagnetization of studied samples and was only capable of unblocking the secondary NRM component. Accordingly, progressive thermal demagnetization was chosen for the entire collection of Telemark samples. ChRM carried by hematite was normally demagnetized by heating to 650–690 °C. Paleomagnetic data from 11 sites were rejected because of either chaotic demagnetization behavior (nine sites) or $\alpha_{95} > 15°$ (two sites). Samples from 8 and 15 sites from the Telemark LU volcanics yielded well-defined ChRM directions of normal NW (negative inclination) and reverse SE (positive inclination) polarity with intermediate to steep inclinations (Table 3). In some samples, NRM resided in both magnetite and hematite (Fig. 8b, d). Both magnetite and hematite remanences have indistinguishable directions with a straight linear trend to the origin of the vector endpoint diagrams (Fig. 8b, d). The

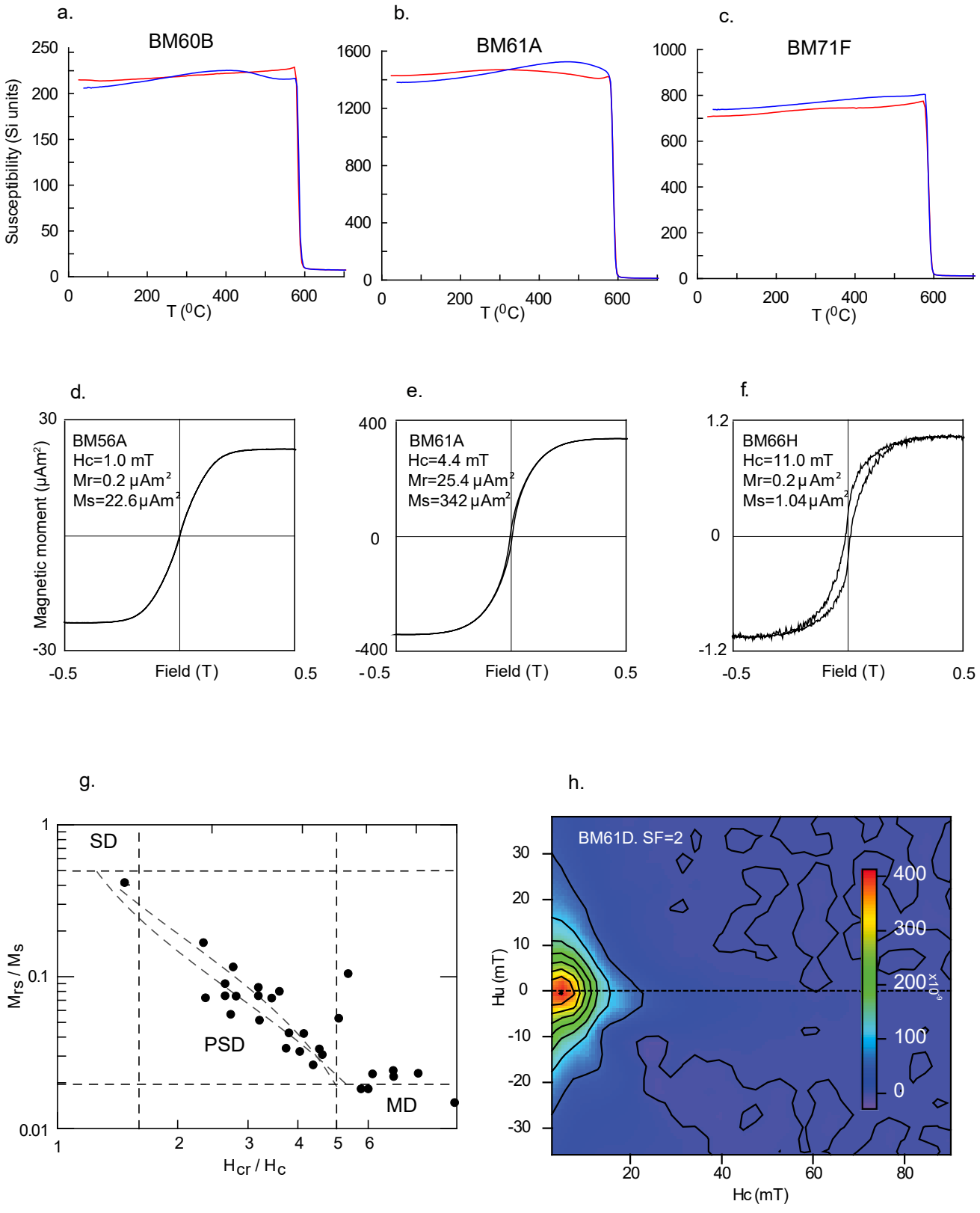

Fig. 6. Rock magnetic properties of mafic xenoliths from the Sirdal Magmatic Belt. (a-c): Typical dependence of low-field magnetic susceptibility (κ) versus temperature showing heating (red curves) and cooling (blue curves); **(d-f)**: Typical magnetic hysteresis loops after paramagnetic slope correction; **(g),** Day plot (Day et al., 1977); (h), First-order reversal curve (FORC) diagram. Abbreviations and other details are the same as in Fig. 3.

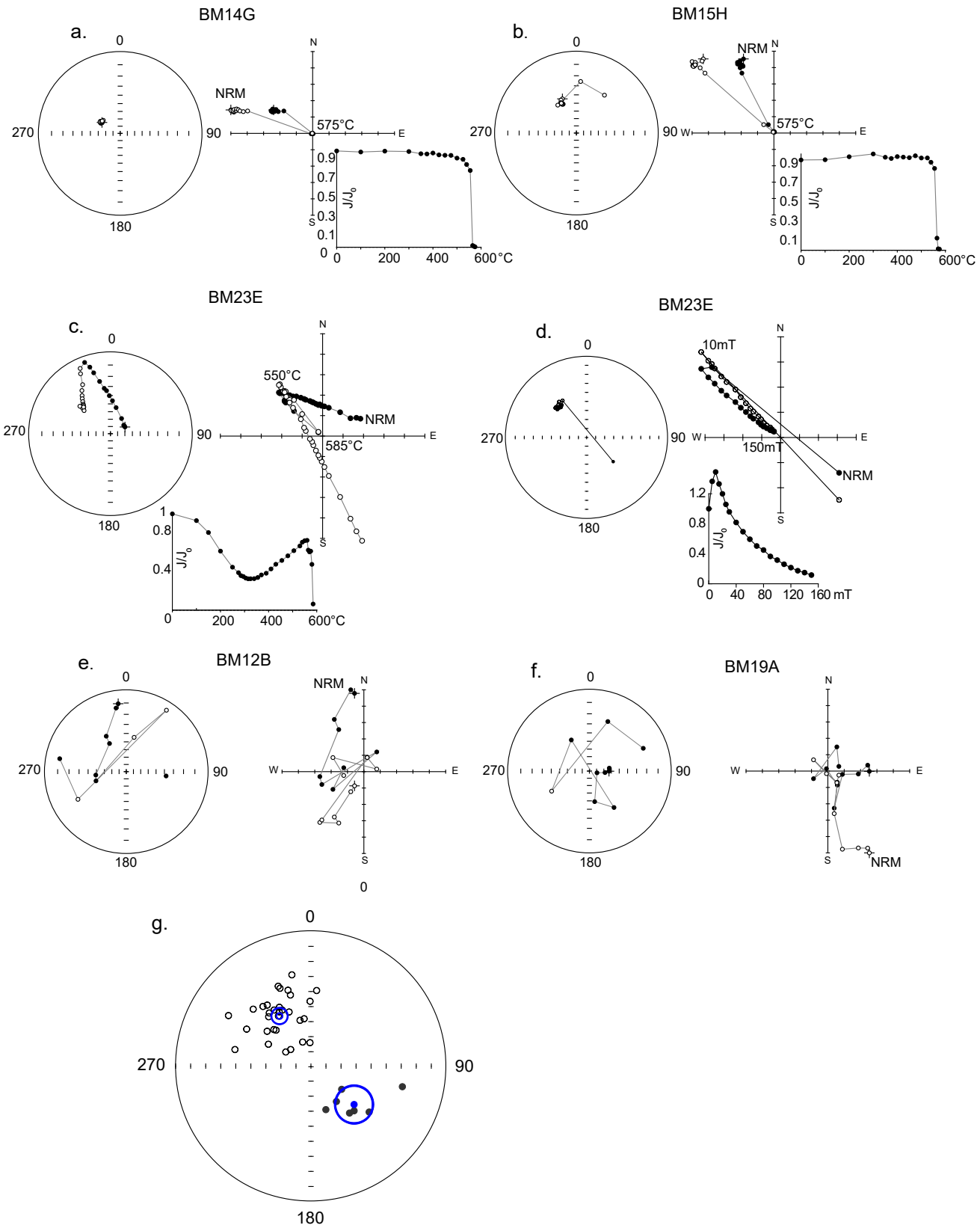

Fig. 7. Paleomagnetism of Bamble rocks. (a-d), Examples of vector endpoint diagrams (open symbols are data-point projections on a vertical plane; solid symbols are projections on a horizontal plane), equal-area projections, and magnetic intensity decay diagrams (normalized natural remanent magnetization versus temperature or applied alternating field); **(e, f)** examples of erratic demagnetization behavior; **(g)** equal-area projection showing paleomagnetic site-mean directions and grand-mean directions with associated 95% confidence circles (α_{95}) for the Bamble lithotectonic unit.

Table 2

Summary of paleomagnetic data for the Bamble Lithotectonic unit. Notes: N_{PC}/N_{GC} number of individual samples' linear principle components/great circles used to calculate the site-mean paleomagnetic direction. S_{lat} and S_{long} indicate sampling sites' coordinates in degrees north and east, respectively. D and I are the calculated paleomagnetic declination and inclination; α95 and k are the 95% confidence circle and the concentration parameter for paleomagnetic directions (Fisher, 1953); Plat and Plong, latitude and longitude of virtual geomagnetic poles (VGPs); A_{95} and K are the 95% confidence circle and the concentration parameter for VGP distribution. N and R indicate normal and reversed polarity of the site (group) mean paleomagnetic directions, respectively. * - paleomagnetic directions from Stearn and Piper (1984) for the Bamble Lithotectonic unit intrusions. [1] – site-mean paleomagnetic directions, calculated from low temperature (coercivity) NRM component, which was typically antiparallel to the characteristic NRM.

Site #	S_{lat}	S_{long}	N_{PC}/N_{GC}	D (°)	I (°)	α95 (°)	k	P_{lat} (°N)	P_{long} (°E)
BM14	59.022	9.541	6/0	314.6	−55.4	7	92.3	−12.2	225.7
BM15	59.031	9.533	7/0	338	−51.2	5.6	117.2	−2.7	208.1
BM17	58.887	9.420	6/0	309.3	−72.6	6.8	97.2	−33.5	218.9
BM18	58.887	9.421	6/0	299.9	−40.7	12.7	28.7	−5.8	242.6
BM20	58.882	9.410	7/0	102.7	27.7	14.4	19	−6.2	261.0
BM21	58.871	9.353	5/0	282.3	−38.3	8.5	81.2	−12.2	257.8
BM23	58.950	9.450	5/0	351.8	−58.2	9.8	61.3	−8.1	195.9
BM23_LC	58.950	9.450	0/7	144.3	61	3.9		−15.2	216.1
BM24	58.941	9.432	4/0	346.6	−58.7	5	335.9	−9.0	199.9
BM24_LC	58.941	9.432	0/3	161.1	59.4	1.1		−10.4	204.0
BM25	58.940	9.429	5/0	314.6	−36.1	13.1	34.8	2.7	231.5
BM26	58.942	9.430	5/0	301.5	−55.6	14.3	29.6	−16.7	235.3
BM32	58.730	9.181	5/0	136	48.7	14.7	27.9	−5.6	226.5
BM38	58.533	8.941	3/0	357.6	−74.4	10.5	138.4	−29.4	190.3
BM39	58.522	8.914	8/0	341	−73.1	4.7	140.4	−28.2	200.0
112*	59.015	9.517	6/0	4.3	−39.6	5.6	103	8.4	185.5
113*	59.015	9.517	6/0	321.2	−39.1	7.1	64	2.8	225.1
115*	59.015	9.517	6/0	332.9	−48.2	4.3	174	−1.1	212.9
116*	59.015	9.517	6/0	337.7	−32.6	11.2	26	11.1	211.1
118*	59.015	9.517	6/0	324.4	−40.1	8.0	51	3.0	222.0
119*	59.015	9.517	6/0	319.4	−46.8	10.1	32	−3.3	224.6
123*	58.896	9.524	6/0	299.3	−70.8	11.2	26	−33.9	226.4
130*	58.903	9.524	7/0	348.2	−28	7.6	48	15.6	201.4
132*	58.903	9.524	7/0	343.9	−40.8	12.8	20	6.7	204.4
136*	58.944	9.489	6/0	297.2	−58.2	8.6	44	−20.7	237.2
137*	58.944	9.489	5/0	315.9	−56.7	10.2	38	−12.9	224.1
138*	58.944	9.489	7/0	343.2	−37.3	6.4	68	9.0	205.4
139*	58.944	9.489	7/0	359.2	−46.9	2.3	511	2.9	190.2
141*	58.946	9.446	7/0	327	−50.3	3.2	273	−4.1	217.3
142*	58.946	9.446	6/0	331.8	−45.6	5.7	102	0.9	214.3
144*	58.946	9.446	6/0	329.7	−48.2	9.7	35	−1.7	215.6
145*	58.946	9.446	5/0	140.6	49.6	15.0	17	−5.2	222.8
148*	58.946	9.446	3/0	338.3	−34.3	8.6	88	10.2	210.3
149*	58.946	9.446	5/0	308.5	−52.8	8.9	50	−11.7	231.3
150*	58.946	9.446	6/0	326.7	−45.4	9.8	34	−0.2	218.8
151*	58.946	9.446	4/0	321.9	−45.1	9.5	54	−1.2	222.9
153*	58.808	9.319	5/0	128.3	40.7	8.2	58	−2.5	235.5
154*	58.808	9.319	4/0	127.1	64.4	10.8	42	−23.7	226.4
Mean N			31	327.9	−50.7	5.7	21.3	−5.8 A_{95} = 6.8°	216.3 K = 15.5
Mean R			7	131.7	51.6	13.3	21.6	−10.2 A_{95} = 14.4°	227.4 K = 18.4
Mean N + R			**38**					**−6.6** **A_{95} = 6.1°**	**218.4** **K = 15.6**

accepted group-mean paleomagnetic directions (D = 315.8°, I = -59.8°, α_{95} = 8.8°, k = 48.8, N = 8 and D = 120.5°, I = 55.2°, α_{95} = 6.4°, k = 37.4, N = 15) pass the reversal test of McFadden and McElhinny (1990) in classification '*B*' with the observed angle between the directions (when one group mean is inverted) γ = 9.4° and critical angle γ_c = 10.2°. To avluate the age of magnetization with respect to that of folding, which is somewhat tentatively constrained at < 1145 Ma, we conducted the fold test of Watson and Enkin (1993). The results of the fold test indicate that the best grouping of site-mean paleomagnetic directions is achieved at 13.1 ± 4.1% of unfolding (Fig. 8h) suggesting a late *syn*-folding age of measured magnetization. The direction-correction (DC) test of Enkin (2003) yielded negative results with 16.3 ± 18.4% of optimal unfolding for measured paleomagnetic directions, indicating a post-folding age of magnetic remanence in the studied rocks. Finally, the McFadden and Jones (1981) fold test, which instead of probing the clustering of paleomagnetic direction as a function of untilting degree tests the hypothesis of whether the tilt-corrected directions for the two-fold limbs can be considered as drawn from the same distribution of directions, indicates that the null-hypothesis can be rejected at 95% confidence and magnetization is more likely to be of post-folding origin. Overall, negative fold tests imply a post-folding age of magnetization. The corresponding mean VGPs, calculated using uncorrected site-mean directions, are located at P_{lat} = -17.4° N, P_{long} = 221.3E° E (A_{95} = 10.0 °, K = 31.8) and P_{lat} = -17.3° N, P_{long} = 234.4°E (A_{95} = 8.3 °, K = 22.0). The mean paleomagnetic pole, based on all 23 VGPs is located at P_{lat} = -17.4° N, P_{long} = 229.8° E (A_{95} = 6.5 °, K = 22.6). Similar to the Bamble pole, the new Telemark pole was graded as a 4-point reliability score (Meert et al., 2020).

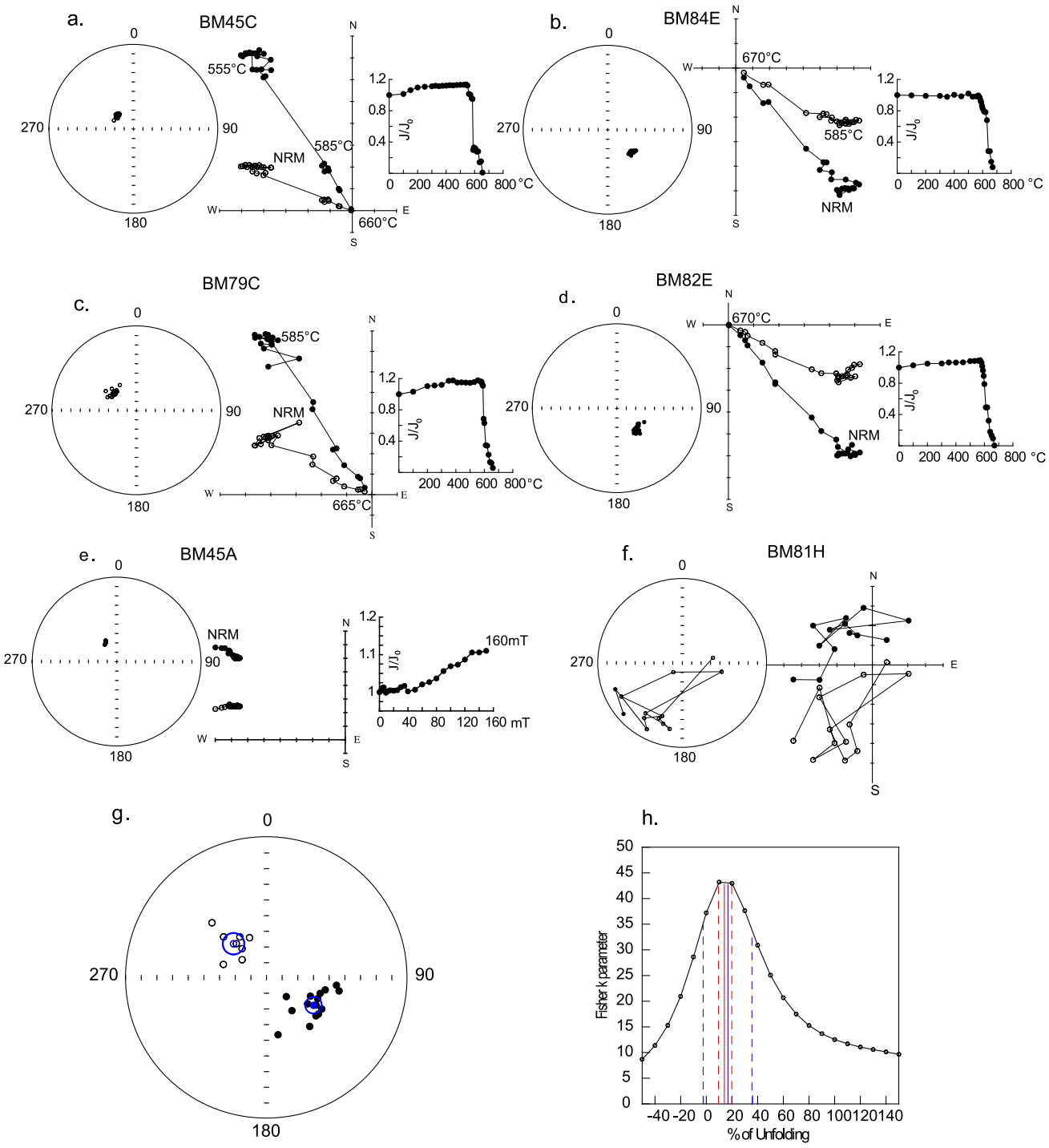

Fig. 8. Paleomagnetism of central Telemark volcanics. (a-d), Examples of vector endpoint diagrams (open symbols are data-point projections on a vertical plane; solid symbols are projections on a horizontal plane), equal-area projections, and magnetic intensity decay diagrams (normalized natural remanent magnetization versus temperature); **(e)** example of alternating field (AF) demagnetization, illustrating that AF demagnetization was not capable of demagnetizing these samples; **(f),** examples of erratic demagnetization behavior; equal-area projection showing paleomagnetic site-mean directions and grand-mean directions with associated 95% confidence circles (α_{95}) for the Telemark volcanics; **(h),** results of the Watson and Enkin (1993) fold test. The solid red line (red dashed lines) shows the maximum k-parameter (Fisher, 1953) degree of untilting (95% confidence bounds). The solid blue line shows the optimal degree of untilting, yielded by the direction-correction fold test (Enkin, 2003) and its 95% confidence limits (blue dashed lines).

4.3.3. Southwestern part of the Telemark lithotectonic unit. Mafic xenoliths within granites of the Sirdal Magmatic Belt

The majority of samples from the SMB mafic xenoliths manifested a well-defined characteristic NRM component (Fig. 9a–c) with rather narrow unblocking temperature spectra of ~ 570–590 °C, characteristic of magnetite after a noisy secondary overprint was removed by heating to 350–450 °C. Data from nearly 30% of the samples were rejected partly due to erratic demagnetization trajectories (three sites) and partly because of large radii of the 95% confidence circle $\alpha_{95} > 15^{\circ}$ (three sites). Characteristic remanent magnetization components typically have very steep negative inclinations and generally NW–NNW-directed declinations. Accepted paleomagnetic data from samples from nine sites

Table 3
Summary of paleomagnetic data for the central Telemark volcanics. Notes are similar to those for Table 2, except for N, which indicates the number of samples' individual principle components (linear fits). No great circle-type demagnetization paths were observed.

Site	S_{lat}	S_{long}	N_{PC}	D (°)	I (°)	α95 (°)	k	P_{lat} (°N)	P_{long} (°E)
BM45	59.356	8.238	8	306.3	−70.7	10.7	27.6	−32.1	221.3
BM46	59.356	8.238	8	337	−62.3	5.9	88.6	−14.7	205.2
BM48	59.452	8.351	6	112.9	59.6	8.7	59.9	−24.1	238.5
BM49	59.451	8.337	7	137.2	71.4	10.8	32.0	−30.4	214.4
BM50	59.496	8.179	6	318.4	−61	15	20.9	−17.2	219.2
BM51	59.423	7.978	6	125	49.5	9.1	55.0	−10.6	234.0
BM76	59.697	8.050	5	315.2	−40.6	6.7	132.4	−0.6	228.4
BM79	59.329	8.372	4	313.5	−52.2	12	59.1	−9.8	226.6
BM82	59.530	8.091	8	138.5	48.4	5.7	96.0	−5.1	223.6
BM83	59.357	8.218	8	142.4	63.4	5.5	101.4	−18.8	215.4
BM84	59.356	8.217	8	119.6	49.4	8.5	43.0	−12.5	238.5
BM85	59.422	7.977	8	106.4	54.3	2.7	424.4	−22.0	246.1
BM86	59.420	7.975	7	119	53.8	12	26.3	−16.4	236.8
BM87	59.420	7.973	9	96.2	45.1	5.7	83.3	−19.7	258.7
BM88	59.414	7.965	8	100.4	42.9	5.1	117.2	−16.2	256.2
BM89	59.375	7.842	7	122.5	58.9	6.3	93.8	−19.8	231.5
BM90	59.375	7.842	8	168.6	52.8	9.3	36.7	−3.2	197.4
BM91	59.375	7.843	7	112.4	54.7	6.4	89.2	−19.7	241.2
BM92	59.375	7.843	8	101.8	51.7	9.7	33.6	−21.9	250.9
BM93	59.351	8.210	4	287	−61.2	7.1	167.3	−27.9	241.4
BM94	59.351	8.220	9	326.8	−58.9	6.8	59.0	−12.7	213.8
BM95	59.490	8.260	4	127.7	50.1	2.6	724.9	−10.1	231.9
BM96	59.490	8.260	9	319.9	−65.8	12.8	17.0	−22.4	216.0
Mean N			8	315.8	−59.8	8.0	48.8	−17.4 A_{95} = 10.0°	221.3 K = 31.8
Mean R			15	120.5	55.2	6.4	37.3	−17.3 A_{95} = 8.3°	234.4 K = 22.0
Mean N + R			**23**					**−17.4** **A_{95} = 6.5°**	**229.8** **K = 22.6**

(Table 4) resulted in mean paleomagnetic direction D = 303.6°, I = -80.6°, α_{95} = 6.4°, k = 64.9 and the associated mean virtual geomagnetic pole was calculated at P_{lat} = -46.2° N, P_{long} = 209.4° E (A_{95} = 12.0, K = 19.4, N = 9). This pole merits a 3-point on the reliability R-score scale (Meert et al., 2020).

5. Discussion

5.1. Geochronology, rock magnetism, and the age of natural remanent magnetization

Estimating the age of natural remanent magnetization in metamorphic rocks is not a trivial task and requires a robust understanding of the cooling history of rocks, their magnetic mineralogy, and NRM blocking temperatures (T_b). Rocks subjected to high-grade metamorphism usually acquire 'new' magnetization, which is then blocked during post-peak metamorphic cooling. This cooling is a process that occurs on time scales of thousands to tens of millions of years. Accordingly, when dealing with the paleomagnetism of high-grade metamorphic rocks, thorough scrutiny of NRM blocking temperatures and age is required. The (un)blocking temperatures, their spectra, and, eventually, the timing of remanence acquisition intrinsically depend on magnetic mineralogy, i.e., specific NRM carriers and their chemical composition, mixtures, domain state, etc. For instance, NRM in magnetite, characterized by a blocking temperature (T_b) of ~ 400 °C, will be completely reset during prolonged heating to 250–300 °C (Pullaiah et al., 1975), whereas magnetization with T_b near the Curie point is practically time-insensitive and will survive prolonged exposure to even greater temperatures. For the magnetite–ulvöspinel series, the blocking temperatures are controlled by degrees of oxidation and exsolution. In high-grade metamorphic rocks, high-temperature oxidation and exsolution occur at temperatures well above the blocking temperatures of magnetic minerals and usually results in intergrowth of ilmenite (or ulvöspinel, later oxidized to ilmenite) lamellae in a Fe-rich, typically nearly stoichiometric magnetite phase (Lindsey, 1991). Brown and McEnroe (2012) in their study of Adirondack high-grade metamorphic rocks showed that ~ 570 °C is a sound estimate for blocking of magnetization in SD–PSD magnetite during post-peak-metamorphism cooling.

For the hematite–ilmenite series, the situation is more complicated. Exsolution, blocking temperatures, and overall magnetic properties in these oxides are controlled by Fe–Ti composition as well as by amount and size of exsolved ilmenite lamellae, which, in turn, depend on the cooling history (Brown and McEnroe, 2012). Hematite-bearing metamorphic rocks often carry chemical or thermochemical remanent magnetization (TCRM) as opposed to magnetite-bearing rocks, which in most cases are characterized by thermal remanence (TRM). (T)CRM acquired during the exsolution process usually has short-term laboratory unblocking temperatures significantly higher than natural acquisition temperatures. Therefore, the use of the laboratory unblocking temperatures as the first-order constraint on T_b may result in erroneous magnetization age estimates. The one-atmosphere hematite–ilmenite phase diagram (Brown and McEnroe, 2012) indicates that hematite with an ilmenite content<15% will block magnetization at temperatures slightly higher than ~ 520 °C, while more ilmenite-rich compositions will acquire magnetization at lower temperatures than the eutectoid point T_e = 520 °C. A detailed overview of magnetic mineralogy, oxidation processes, and NRM acquisition is beyond the scope of this study, and we refer readers to the magnetic mineralogy section in Brown and McEnroe (2012) for further details.

5.1.1. The Bamble lithotectonic unit

The oxide-sulfide textures of the Bamble rocks have been studied extensively (Harlov, 1992, 2000b; Nijland et al., 2014). These studies

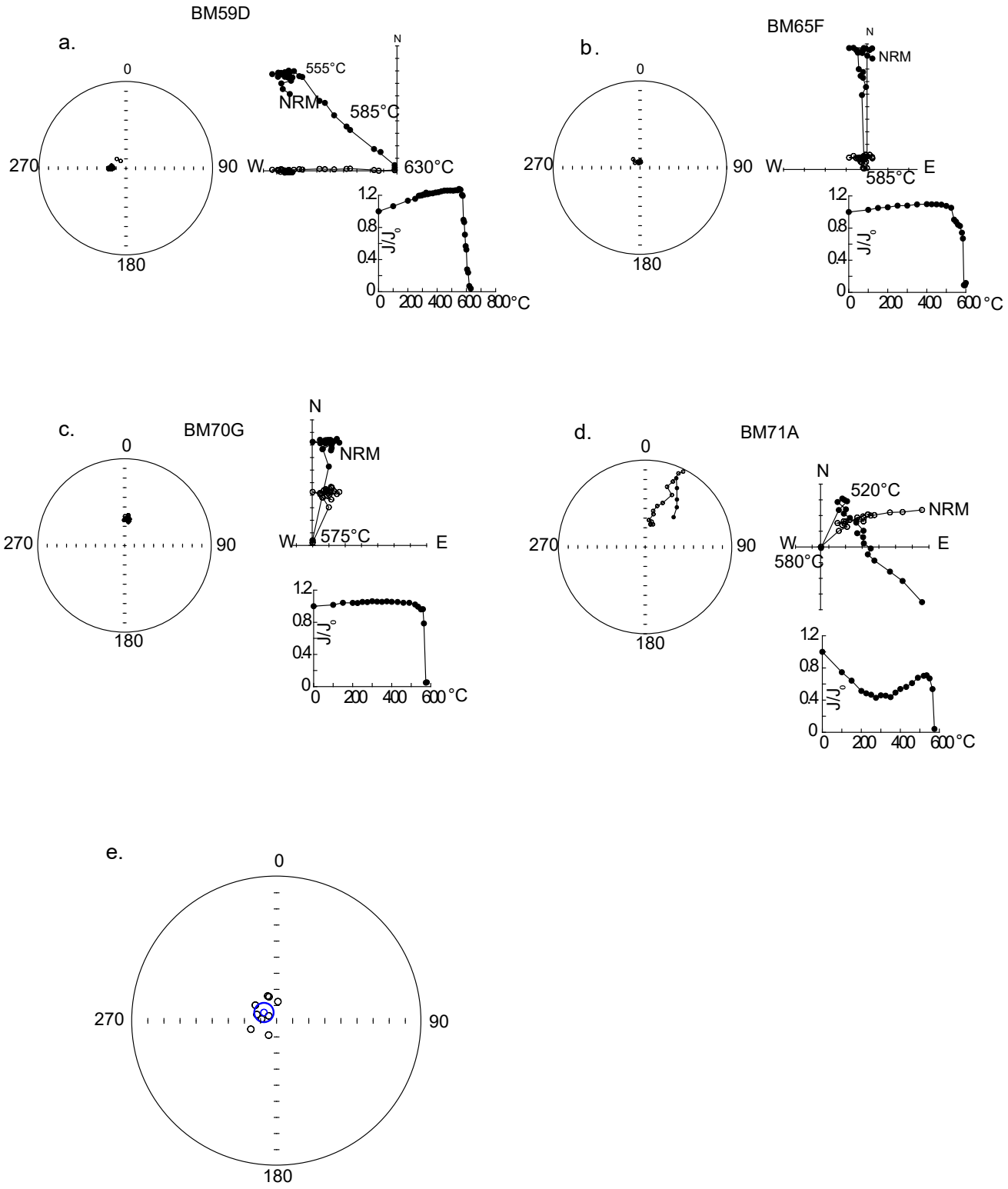

Fig. 9. Paleomagnetism of mafic xenoliths from the Sirdal Magmatic Belt. (a-d), Examples of vector endpoint diagrams (open symbols are data-point projections on a vertical plane; solid symbols are projections on a horizontal plane), equal-area projections, and magnetic intensity decay diagrams (normalized natural remanent magnetization versus temperature or applied alternating field); **(e),** equal-area projection showing paleomagnetic site-mean directions and grand-mean direction with associated 95% confidence circle (α_{95}) for the mafic xenoliths from the Sirdal Magmatic Belt.

indicate that primary oxides in high-grade Bamble rocks are typically magnetite and titanomagnetite with varying degrees of high-temperature oxidation resulting in exsolution of ulvöspinel/ilmenite lamellae in magnetite. The Fe–Ti oxides of the hemo-ilmenite series are also present, yet less abundant. Titaniferous magnetite appears to outnumber hemo-ilmenite by at least a factor of four (Nijland et al., 2014). Rocks that contain sulfides typically have pyrrhotite as a principal sulfide phase (Harlov, 1992, 2000b). Consistent with the previous studies, our rock magnetic and SEM analyses indicate that magnetite in its high-temperature oxidation state and pyrrhotite are the main oxide

Table 4
Summary of paleomagnetic data for the mafic xenoliths from the Sirdal Magmatic Belt. Notes are similar to those for Table 2.

Site	S_{lat}	S_{long}	N_{PC}	D (°)	I (°)	α95 (°)	k	P_{lat} (°N)	P_{long} (°E)
BM56	58.589	7.794	3	340.4	−73.6	4.9	638.7	−29.1	199.0
BM58	58.879	7.871	6	342.6	−74.3	10.2	44.2	−30.3	197.6
BM59	58.600	7.880	8	287.9	−77.2	2.2	650.4	−45.3	221.9
BM60	58.600	7.880	4	4.0	−78.0	8.2	127.1	−35.6	186.0
BM62	58.613	6.903	6	306.5	−73.6	5.9	128.7	−35.3	216.9
BM64	58.540	6.940	4	302.8	−84.2	7.3	188.6	−51.2	202.4
BM65	58.524	6.937	9	277.4	−80.7	11.8	20.0	−52.1	217.1
BM66	58.266	7.217	3	252.0	−73.2	10.2	72.5	−54.3	244.6
BM72	58.25‘	7.191	5	209.1	−79.9	9.0	73.4	−72.8	220.7
Mean			9	303.6	−80.6	6.4	64.9	**−46.2** **A_{95} = 12.0°**	**209.4** **K = 19.4**

and sulfide in studies rocks, respectively. Our results revealed an obvious correlation between the Bamble samples' rock magnetic properties and particular lithologies. For example, all samples from post-tectonic granites that consistently yielded typical MD magnetic hysteresis parameters failed to provide interpretable demagnetization data. In addition, the majority of samples characterized by the presence of a significant amount of pyrrhotite detected during thermomagnetic analyses, yielded erratic and uninterpretable demagnetization trajectories, whereas those with no pyrrhotite content or a relatively small amount of Fe-sulfide, observed as minor inflections in the thermomagnetic curves, usually gave good-quality demagnetization data. The overall rock-magnetic characteristics of Bamble samples indicate that all accepted paleomagnetic data were obtained from PSD–SD magnetite with narrow unblocking temperature spectra close to the Curie points of magnetic minerals, implying that the high-temperature/coercivity characteristic remanence was blocked by gabbros and amphibolites of the Bamble LU during post-peak metamorphism regional cooling when temperatures reached ~ <570 °C.

Ample geochronology data on metamorphism and cooling of the Bamble rocks indicate that the high-grade metamorphism with associated temperatures of ≥ 750–700 °C peaked at ~ 1140 Ma (e.g., Bingen et al., 2008a). A U–Pb age of 1104 ± 7 Ma, measured from metamorphic zircon from scapolite gabbro in the NE part of the Bamble LU near Ødegården Verk (Slagstad et al., 2020) indicates a younger metamorphic event, likely related to the onset of metasomatic activity in the area. The same gabbro yielded 1090–1084 Ma U–Pb rutile ages, interpreted as indicative of regional cooling that occurred contemporaneously or following high-temperature metasomatism (Engvik et al., 2011). Based on the analyses of new and previously published U–Pb zircon, titanite, and rutile ages, $^{40}Ar/^{39}Ar$ hornblende, biotite, plagioclase as well as Rb–Sr phlogopite age data (Bingen et al., 2008b, Engvik et al., 2011; Cosca and O'Nions, 1994, Cosca et al., 1998), Slagstad et al. (2020) suggested that the Bamble rocks experienced a rather fast cooling from ~ 700 °C at ~ 1104 Ma to 400–450 °C by ~ 1080 Ma. This translates to cooling rates of approximately 8–12.5 °C/Myr. Given the estimated cooling rates, the Bamble LU rocks cooled through ~ 570 °C

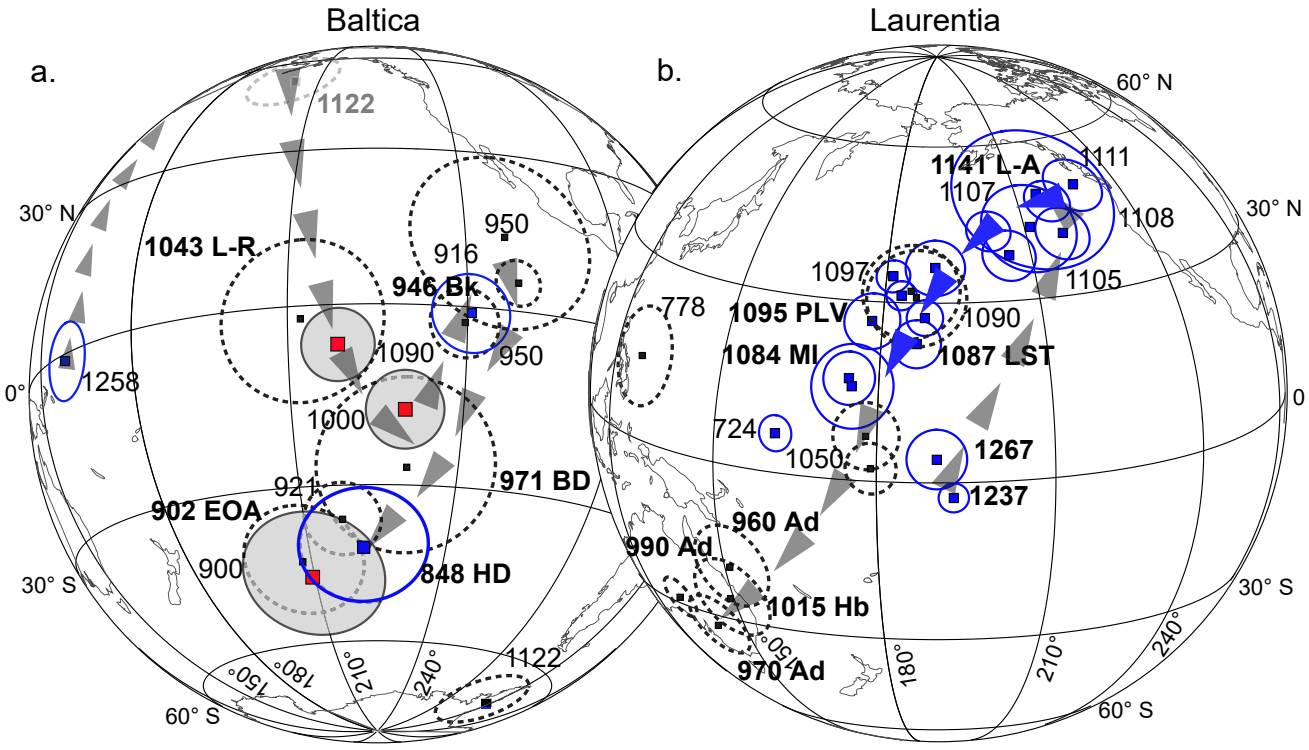

Fig. 10. Apparent polar wanderer paths (APWPs). (a) - for Baltica and **(b) -** for Laurentia with associated 95% confidence ovals (A_{95}s). Blue poles with blue A_{95}s are A-grade poles (see text and Evans et al., 2021). Black poles with A_{95}s shown as dashed lines are B-grade poles of Evans et al. (2021) and poles that have no grades but are listed in Table 5. Red poles with grey-shaded A_{95}s are paleomagnetic poles reported in this study. Numbers next to the poles indicate poles' age in Myr. Letters next to pole ages indicate paleomagnetic poles discussed in the text.

temperatures by 1095–1085 Ma and the new Bamble paleomagnetic pole can be assigned this age.

The positive reversal test supports the "primary" origin of magnetization, acquired during the post-peak-metamorphism cooling of Bamble rocks. In addition, many samples manifested NRM consisting of two oppositely directed components. Isolated in both thermal and alternating field demagnetizations, this dual-polarity is highly unlikely to be an artifact and indicates that the NRM in these rocks was blocked during cooling through a geomagnetic reversal. These observations imply that the high-temperature magnetic remanence measured from the Bamble samples faithfully record paleosecular variations of the geomagnetic field. The new paleomagnetic pole is located close to and within the A_{95} of the mean VGP obtained from Laanila–Ristijarvi dikes (1043 L-R pole in Fig. 10a). The positive baked-contact test validated the primary NRM nature in these dikes (Mertanen et al., 1996). The Laanila–Ristijarvi dikes yielded a rather imprecise Sm-Nd age of 1043 ± 50 Ma, the upper limit of which is consistent with our age estimates for the Bamble pole.

5.1.2. Central part of the Telemark lithotectonic Unit. The Telemark sector

In general, the central part of the Telemark LU has received far less attention than the western SNO and the adjacent Bamble LU, both with regard to geochronology and paleomagnetism. Except for one dubious paleomagnetic pole (Piper, 2009) of highly uncertain age from the Telemark gneisses and quartzites, no data have been reported for the Telemark sector. In this study, we focus on the volcanic rocks of the Telemark sector supracrustals, which have greater potential to retain paleomagnetic signals and provide good quality paleomagnetic data, than gneisses and quartzites.

Rock magnetic analyses of the Telemark volcanics showed that SD hematite is the principal magnetic phase (Fig. 4) in the studied samples. In a few cases, hematite co-exists with lesser amounts of magnetite. The FORC diagrams indicate that magnetite, where present, is in a PSD magnetic state, while hematite is exclusively in the SD state (Supplementary Figure S2). Characteristic NRM is mainly carried by high-coercivity/temperature minerals (Fig. 7) with unblocking temperatures typical for hematite. Although in some samples a small portion of the ChRM resides in magnetite, most of the NRM was demagnetized by temperatures around 630–670 °C. Both magnetite and hematite components are characterized by indistinguishable paleomagnetic directions. The SEM study of magnetic mineral textures reveals well-established ilmenite lamellae within hematite grains, which suggest blocking of the (T)CRM by these grains at about 520 °C (Brown and McEnroe, 2012).

Geochronology data for the Telemark sector and particularly for the Telemark supracrustals are limited to a few U–Pb determinations, which range between 1155 and 1145 Ma (Laajoki et al., 2002) and provide temporal constraints on the age of deposition and emplacement of the central Telemark sedimentary and volcanic sequences. Cooling ages for the Telemark sector rocks are absent. This makes estimations of the magnetic remanence age in the studied rocks challenging. Our results from $^{40}Ar/^{39}Ar$ geochronology are, therefore, a significant contribution to the geochronology data for the SNO in general, and for the Telemark LU, in particular. The studied samples yielded consistent hornblende ages of 1008 ± 22 and 1023 ± 5 Ma, from two different samples and a single biotite age of 961 ± 13 Ma. Although tentative, these data indicate cooling of the Telemark supracrustals from ~ 550–530 °C to 350–330 °C at rates in a range between approximately 2.5 and 5 °C per Myr. Such cooling rate suggests blocking of magnetic remanence by hematite at ~ 520 °C by ~ 1000 Ma. Accordingly, the new paleomagnetic pole for the Telemark lithotectonic unit is assigned an age of ~ 1000 Ma. The age estimate is broadly consistent with the results of the fold tests, which indicate a post-folding age of magnetic remanence, acquired after the ~ 1145 Ma youngest tilting of the Telemark supracrustals.

The new pole is statistically different from the older Bamble and the younger ~ 946 Ma Blekinge Dolerite dikes pole in Sweden (pole 946 Bk in Fig. 10 a, Pisarevsky and Bylund, 2006; Gong et al., 2018) and fills a ~ 150 Myr gap in the Baltican APWP between 1090 and 940 Ma. The new pole plots close to and within the relatively large $A_{95} = 14.9°$ of the 971 ± 7 Ma mean VGP obtained from the Blekinge-Dalarna dikes (pole 971 BD in Fig. 10a), primary nature of which was confirmed by a positive baked-contact test (Gong et al., 2018). The positive reversal test, proximity to the primary ~ 971 Ma pole, and the large number of individual VGPs used in the paleomagnetic pole calculation strongly suggest that the new Telemark pole is based on magnetization acquired by the studied rocks during regional cooling at ca. 1000 Ma and adequately reflects the time-averaged geomagnetic field at this time.

5.1.3. Southwestern part of the Telemark lithotectonic unit. Mafic xenoliths within granites of the Sirdal Magmatic Belt

The SMB xenolith samples are characterized by PSD to MD magnetite as a principal magnetic mineral. Consistent with our rock magnetic analyses, characteristic NRM components measured from the SMB xenolith samples are usually unblocked by temperatures ranging between 570 and 590 °C, typical of magnetite. SEM images indicate that magnetic grains within mafic xenoliths underwent high-temperature oxidation and have rather irregular intergrowths of a Ti-rich phase within Ti-poor magnetic titanomagnetite. However, the EDS spectra of the Ti-poor magnetic phase suggest incomplete unmixing of titanomagnetite with a substantial amount of Ti remaining in the Fe-richer (Ti-poor) phase. The observed textures correspond to high-temperature oxidation stage II, according to Haggerty (1991).

The accepted ChRM components have steep, generally NNW-directed normal-polarity (negative inclination) directions. $^{40}Ar/^{39}Ar$ data obtained from three individual xenoliths yielded hornblende ages ranging between 957 and 910 Ma. Biotite ages measured from the same samples range between 898 and 854 Ma. The spread in ages likely reflects the protracted cooling history of the SMB granites. The use of a widely accepted $^{40}Ar/^{39}Ar$ blocking temperature in hornblende of ~ 550–530 °C indicates that magnetic remanence would be blocked by approximately 930 Ma in the bulk of SMB xenoliths by SD–PSD magnetite-bearing samples. We note, however, that most of the SMB xenoliths studied here are characterized by large PSD to MD magnetite that would likely block NRM at somewhat lower temperatures than SD–PSD systems. Although a precise estimate of the NRM age in our samples is at best difficult, the new paleomagnetic pole is statistically similar to the ~ 900 Ma pole from Egersund–Ogna anorthosite (pole 902 EOA in Fig. 10a, Brown and McEnroe, 2004). The similarity of the paleopole positions suggests that ~ 900 Ma is a sound age estimate for the new paleomagnetic pole.

The NRM nature of the SMB xenoliths is inherently difficult to ascertain due to the lack of paleomagnetic tests. Post-900 Ma remagnetization related to a regional metamorphic hydrothermal event has been proposed based on a paleomagnetic pole obtained from the ~ 850 Ma Hunnedalen dikes (Walderhaug, et al., 1999). This pole resembles 930–900 Ma poles for Baltica. Such a metamorphic event, however, has been questioned by a study of the EOA (Brown and McEnroe, 2004), which showed that the massif anorthosites exposed in the same area with the Hunnedalen dikes lack any secondary alteration. We further note that the ~ 850 Ma pole of Walderhaug et al. (1999) is close, but statistically different from both EOA and the new xenolith ~ 900 Ma pole (pole 848 HD in Fig. 10a). In addition, dikes and measured magnetization are likely slightly older than their 848 ± 27 Ma $^{40}Ar/^{39}Ar$ biotite age, which is close to the $^{40}Ar/^{39}Ar$ biotite ages measured from SMB xenolith samples and probably reflects regional cooling rather than the dikes' crystallization and NRM age. Similar to the SMB xenoliths, the magnetite-bearing Hunnedalen dikes would have blocked magnetization at higher temperatures than ~ 350–330 °C, $^{40}Ar/^{39}Ar$ system closure temperatures in biotite. We also note that the Hunnedalen paleopole is based on paleomagnetic data from six sites that represent four individual dikes and thus may not truly reflect the time-averaged geomagnetic field. On the other hand, the primary nature of the

Hunnedalen dikes mean VGP and its close location to both the EOA and our new xenolith paleomagnetic poles can be used as an argument in favor of the primary nature of the latter two.

5.2. The Proterozoic apparent polar wander path (APWP) for Baltica

Paleomagnetic poles of different age for a continent or a tectonic block are commonly combined into so-called apparent polar wander paths (APWPs) – a convenient way of illustrating the apparent motion of this continent (i.e., the motion of a pole relative to a fixed continent). The Precambrian paleomagnetic database contains approximately 4000 paleomagnetic poles (https://paleomagia.it.helsinki.fi, Veikolainen et al., 2014). However, despite the overall wealth of paleomagnetic data, most of the available poles are of questionable suitability for constructing robust APWPs and paleogeographic reconstructions. The most critical problem with the majority of these data is the lack of robust temporal constraints. Many paleomagnetic poles lack age determinations and were very tentatively dated by fitting to assumed, and, in most cases, ill-defined APW tracks. Given this major uncertainty, a coherent approach is required to select paleomagnetic poles for paleogeographic reconstructions. Under this agenda, a large international group of paleomagnetists discussed and evaluated all published Precambrian paleomagnetic poles during the last three Nordic Paleomagnetic Workshops. The result is a consensus Precambrian dataset (Evans et al., 2021) that contains poles, selected using an agreed set of rigorous acceptance criteria and categorized according to paleomagnetic poles' reliability, including both the traditional paleomagnetic data quality scale of Van der Voo (1990), and the updated set of reliability criteria of Meert et al. (2020). A series of poles referred to as "A-graded" reflects paleomagnetic results that are in structural coherence with the host cratons and have sufficient evidence for being paleomagnetically reliable. This evidence includes paleomagnetic stability tests on the age of magnetization, adequate statistics, and sufficiently precise age constraints. The "B-graded" paleomagnetic poles represent paleomagnetic data that may be considered reliable but do not meet one or more of the aforementioned criteria (Evans et al., 2021). Overall, the new compilation contains 122 and 177 "A" and "B"-graded poles, respectively, representing reliable paleomagnetic data for the entire Precambrian.

The late Meso – to early Neoproterozoic APWP of Baltica has long been debated with regard to both its shape and sense of direction. The new compilation of Precambrian paleomagnetic data for Baltica consists of 12 "A-grade" paleomagnetic poles with only a single ~ 945 Ma pole, representing the time of the SNO tenure (Elming et al., 2014). A total of 40 "B-grade" paleomagnetic poles (Evans et al., 2021) for Baltica (and Baltica–Fennoscandia) includes seven poles for the late pre-SNO to an early post-SNO time interval (between ~ <1200 and 850 Ma, Table 5). These include the early Sveconorwegian mean VGPs from the 1122 ± 3 Ma Salla dike (Salminen et al., 2009), the imprecisely dated (1043 ± 50 Ma) mean VGP pole from the Laanila–Ristijarvi dikes (Mertanen et al., 1996), and the ~ 950 Ma paleomagnetic poles from mafic dikes in southern and central Sweden (Bylund, 1992). The younger Sveconorwegian (~920–850 Ma) paleomagnetic poles are represented by data from various intrusive rocks in SW Norway (Stearn and Piper, 1984; Walderhaug et al., 1999; Brown and McEnroe, 2009, 2015).

Fig. 10a shows paleomagnetic poles (Supplementary table S2), which make a tentative Meso- to Neoproterozoic APWP for Baltica. This APWP is characterized by extremely uneven data distribution and gaps between the consecutive poles, in many cases exceeding 100 Myr. The new paleomagnetic poles presented here contribute to the APWP of Baltica and, importantly, fill the ~ 170 Myr gap between ~ 1120 and 950 Ma. Unfortunately, despite the addition of new poles, the Baltican polar track still lacks data and has gaps often exceeding 50 Myr.

Table 5
Summary of paleomagnetic poles used for paleogeographic reconstructions shown in Figs. 11 and 12. Notes: Pole Grade – paleomagnetic pole reliability grade (see text and Evans et al., 2021 for details). P_{lat} and P_{long}, latitude and longitude of paleomagnetic poles (VGPs); is the paleomagnetic pole's 95% confidence circle. Q(7) – paleomagnetic data quality score (maximum Q = 7) of Van der Voo (1990).

Continent	Description	Pole Grade	P_{lat} (N)	P_{long} (E)	A_{95} (°)	Q (7)	Nominal age (Ma)	min	max	Reference	Year
Baltica	MEAN post-Jotnian intrusions	A	−1.1	161.2	6.6	6	1258	1246	1270	*LULEÅ WORKING GROUP* (Elming & Mattsson 2001)	*2009*
Baltica	Salla Dike	B	71.0	113.0	8.0	5	1122	1119	1127	Salminen et al.	2009
Baltica	Bamble LU		−6.6	218.4	6.1	5	1090			This study	
Baltica	Central Telemark LU		−17.4	229.8	6.5	5	1000			This study	
Baltica	Western Telemark. Mafic X-liths		−46.2	209.4	12.0	4	900			This study	
Baltica	Dikes of central and southern Sweden	A	−0.9	240.7	6.7	7	945	935	955	Elming et al.	2014
Baltica	Mean 951–935 pole (Swedish dikes)	B	−2.6	239.6	5.8	6	943	935	951	Gong et al.	2018
Baltica	971 Ma mean VGP (Swedish dikes)	B	−27.0	230.4	14.9	4	971	964	978	Gong et al.	2018
Baltica	Egersund-Ogna anorthsite		−41.0	222.0	10.5	4	900			Brown and McEnroe	2004
Baltica	Rogaland Ingenous Complex		−35.9	217.9	5.0	4	916			Brown and McEnroe	2015
Laurentia	Lake Shore Traps	A	23.1	186.4	4.0	6	1087	1085	1089	Kulakov et al.	2013
Laurentia	Portage Lake Volcanics	A	26.7	178.0	4.7	6	1095	1092	1098	Hnat et al.	2006
Laurentia	MEAN Nipigon sills and lavas	A	47.2	217.8	4.0	6	1111	1107	1115	*Mean Palmer 1970; Robertson & Fahrig 1971; Pesonen 1979; Middleton et al. 2004; Borradaile et al. 2006*	
Laurentia	Mean Ontario lamprophyres and Abitibi dykes	A	55.8	220.0	7.3	7	1141	1139	1143	Ernst and Buchan (1993), Piispa et al.	*2018*
Laurentia	Sudbury Dikes Combined	A	−2.5	192.8	2.5	6	1237	1232	1242	Palmer et al. (age: Dudás et al. 1994)	1977
Laurentia	Mackenzie dikes grand mean	A	4.0	190.0	5.0	6	1267	1265	1269	Buchan et al.	2000
Laurentia	Haliburton Intrusions - A comp.	B	−32.6	141.9	6.3	3	1015	1000	1030	Warnock et al. (cooling age)	2000
Laurentia	Adirondack highlands	N/A	−18.4	151.1	10.5	4	990			Brown and McEnroe (cooling age)	2012
Laurentia	Adirondack highlands	N/A	−25.1	149.0	11.6	4	970			Brown and McEnroe (cooling age)	2012
Laurentia	Adirondack highlands	N/A	−28.4	132.7	6.9	4	960			Brown and McEnroe (cooling age)	2012

Notwithstanding the overall poor state of the paleomagnetic dataset for Baltica, the APWP has traditionally been compared to that for Laurentia.

The late pre-Sveconorwegian segment of the Laurentian APWP is defined by two 1267 and 1237 Ma "A-grade" paleomagnetic poles (Evans et al., 2021; Fig. 10b, Supplementary table S2). These poles are followed by a ~ 100 Myr time interval for which no paleomagnetic poles were considered reliable. The younger segment is defined by a series of 15 "A-grade" 1140–1085 Ma poles from extrusive and intrusive rocks, associated with the development of the North American Midcontinent Rift (MCR) system (Fig. 10b). This high-quality segment of Laurentian APWP, known as the Keweenawan track, contains the ~ 1095 Ma pole (1095 PLV pole in Fig. 10b) from the lava flows of the Portage Lake Volcanics (Hnat et al., 2006) and the 1087 Ma paleomagnetic pole (1087 LST pole in Fig. 10b) derived from the youngest MCR lava flows of the Lake Shore Traps (Kulakov et al., 2013), which are broadly coeval with the 1095–1085 Ma Bamble pole presented here. The high-quality segment of the Laurentian APWP terminates with the ~ 1084 Ma "A-graded" pole from the Michipicoten Island volcanics (1084 MI pole in Fig. 10b, Fairchild et al., 2017), which is followed by a series of ~ 1050–1020 Ma paleomagnetic poles derived from the MCR-related

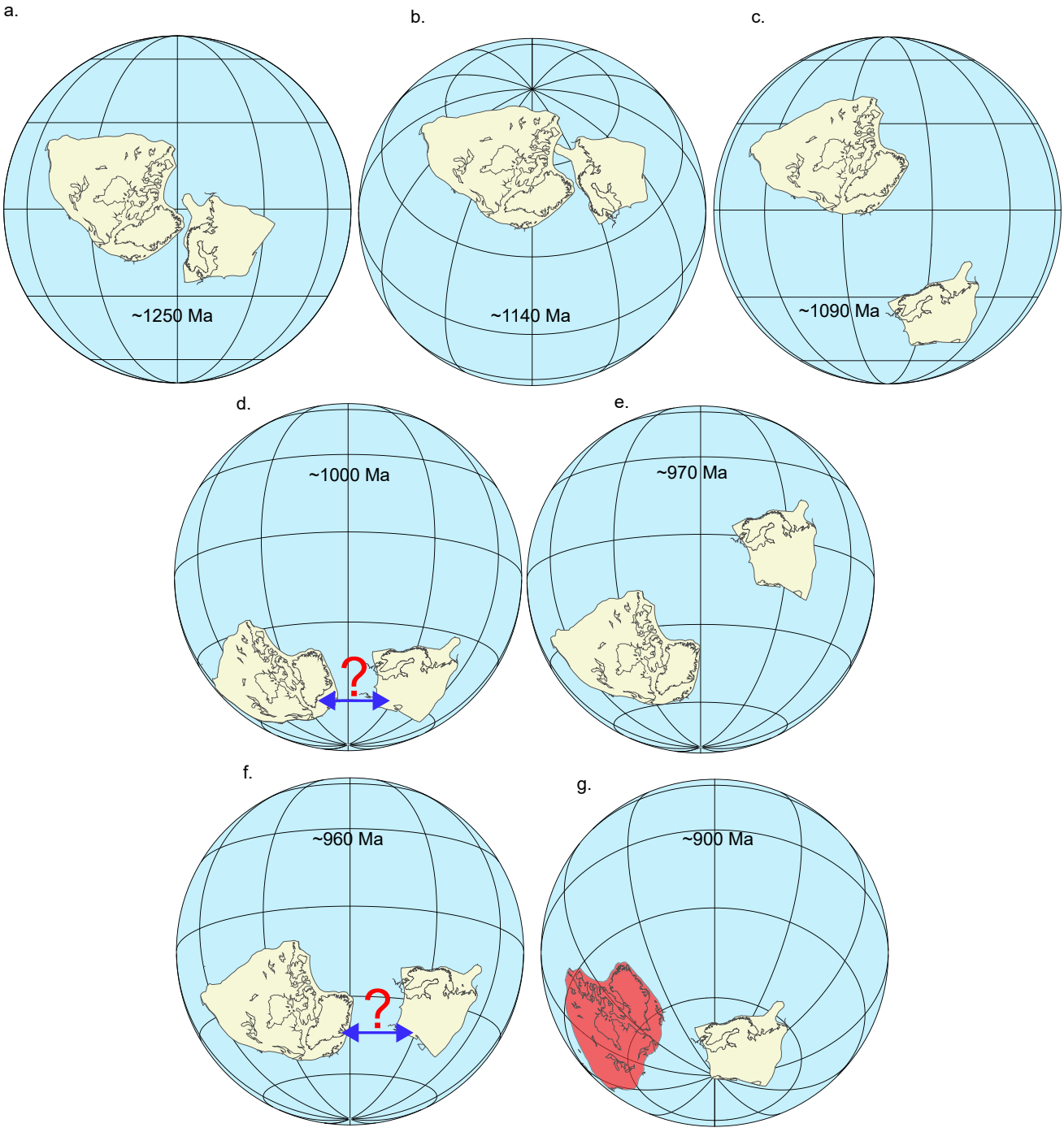

Fig. 11. Paleogeographic reconstructions made using paleomagnetic poles listed in Table 5. Note that paleomagnetism-based reconstructions define latitudinal positions and orientations of continents, but longitudinal positions are arbitrary. Numbers on each reconstruction indicate the age for a particular reconstruction (see text). Blue arrows and a question mark on panels (e) and (f) indicate that longitudinal separation is unknown. (g), Laurentia was shaded in red to illustrate that for ~ 900 Ma no reliable paleomagnetic data for Laurentia exist to constraint its latitude and orientation.

sedimentary rocks with ill-defined ages of deposition and magnetization. No paleomagnetic poles for the time interval between ~ 1015 and 780 Ma have been considered sufficiently reliable and selected for the new compilation (Evans et al., 2021).

Overall, the comparison of the APWPs for Baltica and Laurentia indicates that the paths are only partly coeval and, with exception of ~ 30 Myr represented by the Keweenawan track, are characterized by relatively poor data resolution with major gaps in the paleomagnetic record and sometimes exceeding 100 Myr. This makes direct comparison of individual APWPs problematic at best, or even impossible. Given this situation, the only way to assess and compare latitudinal positions and orientations of Baltica and Laurentia during the late Mesoproterozoic – early Neoproterozoic, is a one-to-one paleomagnetic pole reconstruction comparisons. To do this, we use the set of paleomagnetic poles listed in Table 5. This dataset is largely based on the compilation of Precambrian data of Evans et al. (2021) and the data presented here.

5.3. Paleogeographic implications

An apparently shared Proterozoic tectonic evolution has been used to argue that Baltica and Laurentia were contiguous through much of the Proterozoic. This coevolution, characterized by crustal growth and subsequent reworking along their SW and SE margins, respectively (Condie, 2013; Roberts and Slagstad, 2015), is thought to have culminated during Rodinia supercontinent assembly when the Baltica–Laurentia block collided at ~ 1100–1050 Ma with a third continent, usually inferred to be Amazonia, forming the classical Rodinia core. The timing of assembly, relative positions of these cratons as well as the pre-assembly paleogeography, however, varies much between different Rodinia models (e.g., Pisarevsky et al., 2003; Evans, 2013). While some models assume that Baltica and Laurentia became juxtaposed sometime around ~ 1050 Ma and formed a single entity until at least 850 Ma (Pisarevsky et al., 2003, Li et al., 2008), others have proposed a different scenario in which northern Baltica was juxtaposed with northeastern Laurentia (eastern Greenland, present-day coordinates) before ~ 1250 Ma (Fig. 11a, b) and then rotated clockwise ~ 90° after 1250 Ma (and likely after 1120 Ma) but before 1000 Ma (Cawood et al., 2010). Baltica then remained in its 'secondary' position within Rodinia until the eventual breakup of the supercontinent in the late Neoproterozoic. This 'secondary' Baltica position is nearly identical in most otherwise diverse Rodinia models. Although the Baltica–Laurentia relationship within Rodinia has long been considered the least controversial, the current state of the Precambrian paleomagnetic record does not provide good spatial constraints on the relative latitudinal positions and orientations of Baltica and Laurentia before and during the proposed time of Rodinia tenure. In an attempt to unravel the tangled late Mesoproterozoic–early Neoproterozoic Baltica-Rodinia history, we use existing paleomagnetic data, combined with new paleomagnetic poles reported here. Inferred from paleomagnetism, the paleogeography of Baltica is interpreted here in conjunction with magmatic and metamorphic records for the SNO. These records have been significantly expanded during the last decades and resulted in a better understanding of the tectonic history of Baltica during the development of the SNO.

The ~ 1250–1120 Ma Baltica–Laurentia latitudinal positions and orientations can be assessed using the ~ 1250 Ma "A" and "B-grade" poles listed in Table 5. Accepted in the compilation of reliable paleomagnetic data of Evans et al. (2021), these poles reconstruct Baltica and Laurentia at a similar latitudinal band (Fig. 11a) and allow juxtaposition of Baltica to northern Laurentia at or prior to ~ 1260 Ma (Cawood and Pisarevsky, 2006). Such a configuration is also compatible with geological data (Bingen et al., 2002; Karlstrom et al., 2001).

The 1140–1122 Ma interval is defined by paleomagnetic poles from the Baltican Salla dike (Salminen et al., 2009) Ma and ~ the 1141 Ma Laurentia pole (Piispa et al., 2018) from the Ontario lamprophyre dikes, combined with data from the Abitibi dikes of Ernst and Buchan (1993). We note that although the 1141 Ma pole of Piispa et al. (2018) was not included in the Precambrian dataset because of its more recent publication, it is based on well-dated primary magnetization and comprises sufficient statistics and, therefore, can be considered an "A-grade" pole. The ~ 1140–1120 Baltica–Laurentia configuration is shown in Fig. 11b. We note that the Laurentian and Baltican poles are not exactly coeval and differ by some 20 Myr. However, high-quality paleomagnetic data for Laurentia indicates a polar wander standstill between ~ 1145 and 1110 Ma, implying that the mean ~ 1141 Ma pole of Piispa et al. (2018) reasonably reflects the paleomagnetic pole position for the entire 1140–1110 Ma time interval. We also note that the 1122 Ma Salla dike pole (Salminen et al., 2009) is based on data from a single dike and may not represent the time-averaged geomagnetic field, which in addition to 95% confidence circle $A_{95} = 8°$ provides a lot of freedom for paleogeographic fits.

Paleomagnetic records from Baltica and Laurentia support the model of Cawood et al. (2016) in which Baltica commenced a clockwise rotation at or after ~ 1140–1120 Ma. An over ~ 90° rotation of Baltica relative to Laurentia may have been associated with the opening of the Asgard sea (Cawood et al., 2010; Fig. 11b). Here, however, we propose that Baltica did not remain adjacent to Laurentia but instead rifted and drifted latitudinally (and possibly longitudinally) away from Laurentia. The rift-to-drift scenario is supported by the geological record, which indicates pre ~ 1100 Ma (Puchkov, 2010; Puchkov et al., 2013) rift-related sedimentation and magmatism along the northern margin of Baltica, overlain by the latest Mesoproterozoic to early Neoproterozoic passive-margin successions of cratonic-derived siliciclastic sedimentary rocks (Maslov, 2004; Maslov et al., 1997; Maslov and Isherskaya, 2002; Nikishin et al., 1996; Siedlecka et al., 2004). This scenario is also supported by ~ 1095–1085 Ma paleomagnetic data from both continents. The 1095–1085 Ma Bamble paleomagnetic pole (this study) reconstructs Baltica and Laurentia with a noticeable latitudinal separation between their margins. Regardless of the use of either the ~ 1095 Ma Portage Lake (Hnat et al., 2006) or the ~ 1087 Ma Lake Shore Traps (Kulakov et al., 2013) paleomagnetic poles, the latitudinal separation between the two continents is ~ 30° (Fig. 11c). The cooling history of Bamble rocks, however, may reflect a wide range of ages. We, therefore, tested our Bamble pole-based reconstruction of Baltica against a set of Laurentia paleogeographic positions (Supplementary Figure S5), reconstructed using 1101–1083 Ma paleomagnetic poles from Evans et al. (2021). Regardless of the paleomagnetic pole selection for Laurentia, a significant latitudinal separation between the continental margins remains (Supplementary Figure S5). Such a latitudinal gap allows for the continued presence of an active margin along the SW margin of Fennoscandia during the Sveconorwegian orogeny. This scenario agrees with the SNO geologic record for the ~ 1100–900 Ma period, particularly with regard to the presence of a subduction system and the evolution of the orogen at or behind an active margin (Slagstad et al., 2020). Rifting and drifting of Baltica away from Laurentia theoretically could have occurred sometime between ~ 1250–and 1120 Ma, followed by the post-1120 Ma ~ 90° clockwise spin, but due to the lack of longitudinal constraints, the exact timing and sequence of these events remain largely uncertain.

The ~ 1000 Ma paleomagnetic pole from the Telemark LU (this study) reconstructs Baltica at moderate latitudes between ~ 30°S and 60°S. The latitudinal position of Laurentia can be constrained by the use of the ~ 1015 Ma "B"-graded paleomagnetic pole from the Halliburton intrusions (Warnock et al., 2000), which reconstructs Laurentia with a noticeable latitudinal overlap with Baltica (similar to the 990 Ma reconstruction discussed below). If correct, such Baltica–Laurentia latitudinal relationship would require shifting Baltica away (probably to the east) from Laurentia. We, however, note that the 1015 Ma age of the Haliburton pole is an estimated cooling age (Warnock et al., 2000). ^{40}Ar–^{39}Ar dating of the Haliburton intrusion resulted in hornblende and biotite ages of ~ 990 and 900 Ma, respectively. Depending on multiple factors, the closure temperatures in the Ar-Ar system may vary significantly. We also note that the Haliburton paleomagnetic pole (Pole Hb in

Fig. 10b) does not lie on the younger continuation of the Keweenawan track marked by the poles from Midcontinent Rift sedimentary rocks, but instead plots closer to the younger 990–960 Ma poles from the Adirondacks (Poles 990 Ad, 970 Ad, and 960 Ad in Fig. 10b, Table 5, Brown and McEnroe, 2012). This suggests that magnetization measured from the Haliburton rocks may be significantly younger than 1015 Ma. In addition, the renewed juxtaposition of Laurentia and Baltica at ca. 1000 Ma is at odds with geological data from the SNO; firstly, because orogenic activity started at least 70 Myr earlier and, secondly, because of the well-documented transition from compression to extension at 1000–990 Ma (Slagstad et al., 2020), inconsistent with a collision at this time.

The post-~1000 Ma relative configuration of Laurentia and Baltica is inherently difficult to ascertain. Gong et al. (2018) proposed a scenario in which Baltica and Laurentia were adjacent to each other and drifted from high latitudes towards the equator and back during a relatively short time interval between ~ 990 and 950 Ma. This oscillating motion tentatively interpreted as being caused by an episode of true polar wander. The Gong et al. (2018) model was based on a newly acquired ~ 951–935 Ma paleomagnetic pole and a mean ~ 970 Ma VGP for the Blekinge–Dalarna dolerite dikes in southern Sweden, and a set of 990–960 Ma paleomagnetic poles from high-grade metamorphic rocks from the Adirondack mountains (Brown and McEnroe, 2012). We note, however, that the use of the roughly coeval ~ 1000 Ma paleomagnetic pole from the Telemark volcanics and ~ 990 Ma pole from the Adirondack highlands (Brown and McEnroe, 2012) reconstruct Baltica and Laurentia to an approximately 30–60° latitudinal band with a noticeable latitudinal overlap (Fig. 11d). A similar latitudinal overlap remains in the 960–950 Ma reconstruction (Fig. 11f), made using the 960 Ma Adirondack pole (Brown and McEnroe, 2012) and the ~ 950 Ma pole from the Blekinge–Dalarna dikes (Elming et al, 2014, Gong et al., 2018), while the ~ 970 Ma poles from Baltica and Laurentia (Gong et al., 2018; Brown and McEnroe, 2012), if taken at face value, indicate equatorial latitudes for the former and intermediate to high latitudes for the latter continent (Fig. 11e). In any case, the latitudinal positions of the two blocks for the 990–950 Ma interval do not support the classical Baltica–Laurentia connection at ~ 950 Ma.

While the group of ~ 920–900 Ma paleomagnetic poles from SW Norway (Brown and McEnroe, 2004; 2015, this study) indicates a high-latitude position for Baltica (Fig. 11g), reliable paleomagnetic data for Laurentia are absent. The overall age uncertainties and paucity of paleomagnetic data do not provide any support for the close connection between Baltica and Laurentia at ≤ 950 Ma but, conversely, do not rule it out. The geologic record, however, is more definitive. While there are some similarities in orogenic style between the eastern parts of the Sveconorwegian and central to SW Grenville orogens, particularly with regard to large-scale thrusting and high-pressure metamorphism, the central and western parts of the SNO are remarkably different. Magmatic and metamorphic records there indicate long-lived high-temperature, low- to medium-pressure metamorphism and voluminous granitic magmatism, and the absence of high-pressure metamorphism (Falkum and Petersen, 1980; Slagstad et al., 2018). In addition, except for the Eastern Segment of the SNO, where local thrusting resulted in crustal thickening, the rest of the SNO crust remained thin through the orogeny (Slagstad et al., 2020; Bingen et al., 2018), which one would not expect during a protracted continent–continent collisional orogeny. Extensive research carried out on different parts of the SNO during the last decade has provided a strong case against continent–continent collision as the mechanism behind the Sveconorwegian orogeny (summarized in Slagstad et al., 2020), suggesting instead an active continental-margin arc/back-arc setting. The subduction system was established at least as early as ~ 1040 Ma (Bybee et al., 2014a), but likely significantly earlier (Coint et al., 2015; Slagstad et al., 2020) and operated until at least ~ 950–940 Ma (Corfu, 2019; Slagstad et al., 2020).

In contrast, the geological record from the Grenville province is typically interpreted to reflect orogeny caused by continent–continent collision (Hynes and Rivers et al., 2010, Rivers, 2012; Rivers, 2015), which commenced at ca. 1090 Ma and peaked around 1050 Ma. The colliding continent is typically inferred to have been Amazonia, but supported by rather sparse evidence (McLelland et al., 2013). Reconstructing Amazonia next to SW Baltica and SE Laurentia, however, effectively closes the SW margin of Baltica and is at odds with the geological record in the Sveconorwegian province. The principal differences between the SNO and the Grenville orogen call for an alternative paleogeographic model, different from the classic triple junction Laurentia–Baltica–Amazonia reconstruction. Moreover, if the coeval Grenvillian orogeny was caused by collision with Amazonia, continent–continent collisional models for the SNO require some other, as of yet unrecognized continent.

5.4. Our model.

Our preferred paleogeographic reconstruction assumes a paleogeographic position of Baltica attached to northern Laurentia before 1260 Ma (Cawood and Pisarevsky, 2006). Such a configuration is compatible with geological data (Bingen et al., 2002; Karlstrom et al., 2001) and supported by paleomagnetic data from the two continents. After 1260 and likely after ~ 1120 Ma, Baltica commenced a clockwise rotation that resulted in the opening of the Asgard Sea (Fig. 12a). However, unlike the model of Cawood et al. (2016), we propose that Baltica did not remain adjacent to Laurentia but instead rifted and drifted to higher latitudes. This scenario is supported by ~ 1095–1085 Ma paleomagnetic data from both continents that indicate over 30° latitudinal separation between the Baltican and Laurentian margins and allows for an active margin along the SW Fennoscandia during the Sveconorwegian orogeny (Fig. 12c). We propose that Baltica likely drifted independently and was located farther east from Laurentia between ~ 1050 and 950 Ma. Choosing a more easterly location of Baltica at ca. 1 Ga, allows us to move the Sveconorwegian orogen away from the tectonically contrasting collisional Grenville orogen into the proposed accretionary Valhalla orogen (Fig. 12c–e) or a tectonically similar, but independent active margin.

6. Concluding remarks

New paleomagnetic data for the 1090–1085 Ma period suggest significant latitudinal separation of Baltica and Laurentia at the onset of Sveconorwegian–Grenvillian orogenesis. This observation questions the classical models arguing for a continuous Sveconorwegian–Grenvillian orogenic belt. Paleomagnetic data for younger times (ca. 1000–900 Ma) restore Baltica and Laurentia to similar latitudes, but with orientations and latitudinal positions of potentially conjugate margins that support their independence rather than contiguity. From a geologic perspective, large parts of the Sveconorwegian orogeny, purported to have formed during the continent–continent collision, never underwent significant crustal thickening (e.g., Slagstad et al., 2020). In contrast, the Grenville orogen is characterized by major crustal thickening and development of a wide orogenic plateau (Rivers et al., 2012) and might have started to undergo gravitationally driven extension as early as 1050 Ma (Rivers, 2012), coinciding with the onset of peak granitic volcanism and orogenic activity in the SNO (e.g., Coint et al., 2015). An enigmatic, short pulse of compression in the Grenville at ~ 1005 Ma coincides with a transition from compression to extension in the SNO, thus is also difficult to reconcile with a continent–continent collision at this time. We, therefore, conclude that while Baltica and Laurentia may have resided at broadly similar latitudes between 1000 and 900 Ma, there is no geologic and paleomagnetic evidence for contiguity. If correct, this interpretation supports the observation of Meert (2014b) that there are some strikingly similar configurations of Baltica-Laurentia in many Pangea, Rodinia and Nuna reconstructions. Meert (2014b) introduced the term ‘strange attractor’ for contients assembling and dispersing in

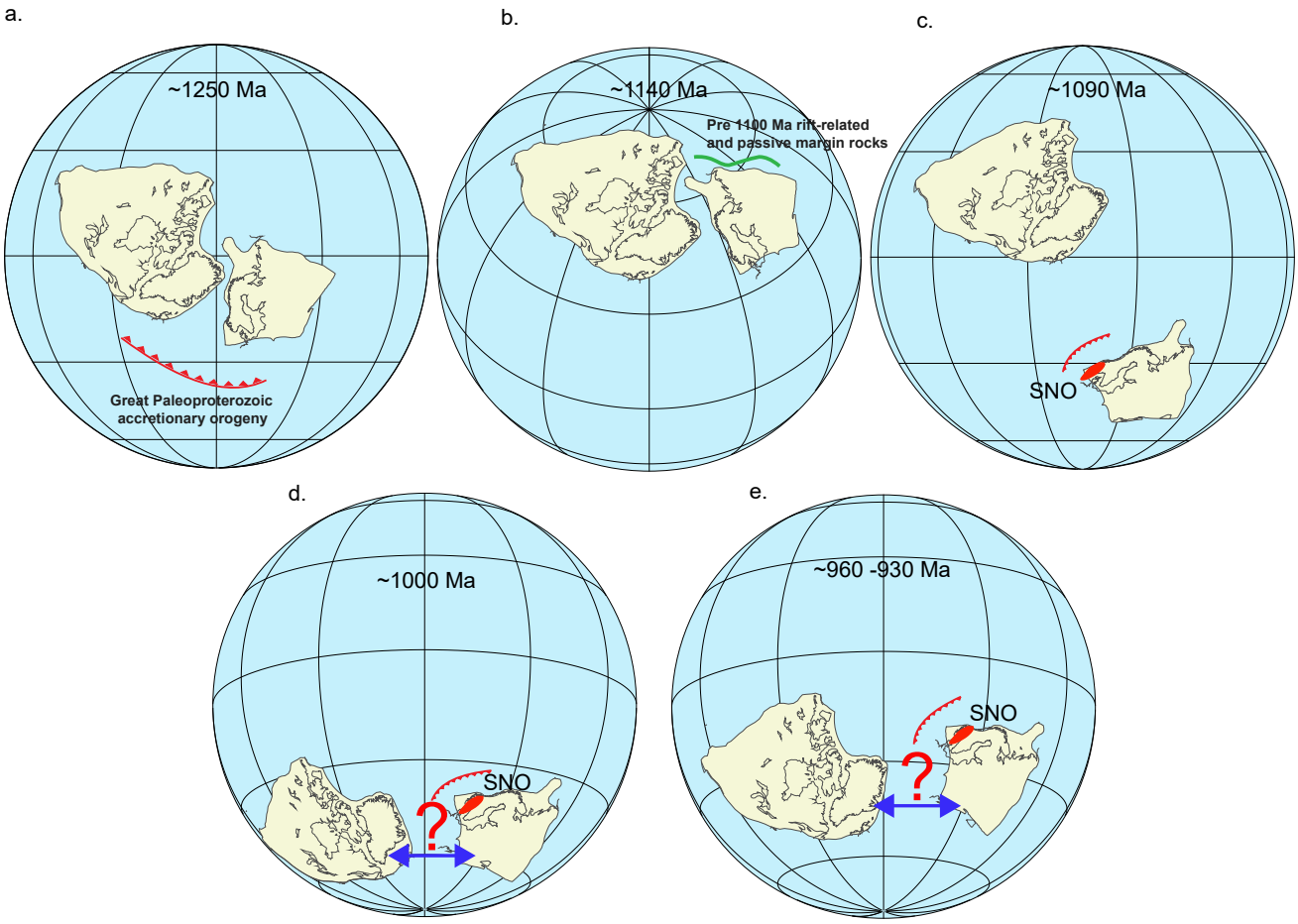

Fig. 12. Paleogeographic model. Our preferred Baltica-Laurentia relationship model for the ~ 1250–930 Ma time interval. Red area at the southwestern (present-day coordinates) part of Baltica schematically shows the Sveconorwegian orogeny. Blue arrows and a question marked on panels (d) and (e) indicate that longitudinal separation is unknown. This model is based on the geological record and supported by available paleomagnetic data (see text).

more or less the same position for billions of years. This is an extreme form of Wilson Cycle tectonic modelling and probably very unikely.

CRediT authorship contribution statement

Evgeniy V. Kulakov: Conceptualization, Investigation, Writing – original draft, Data curation. **Trond Slagstad:** Investigation, Writing – review & editing. **Morgan Ganerød:** Investigation, Writing – review & editing. **Trond H. Torsvik:** Writing – review & editing.

Declaration of Competing Interest

The authors declare that they have no known competing financial interests or personal relationships that could have appeared to influence the work reported in this paper.

Acknowledgments

We thank the Research Council of Norway (RCN) for support through its Centers of Excellence funding scheme (project 223272: CEED). T.S. and M.G. thank the Geological Survey of Norway (NGU) for support. We thank Joeseph Meert, Fernando Corfu, and an anonymous reviewer for their thoughtful reviews. We also thank Pavel Doubrovine, Petter Silkoset, Benjamin Bultel, Mathew Domeier, Alexey Shulgin, Laviniu Gaina, for their help in the field and laboratory.

Data availability

Raw geochronology data are available as a supplementary material table. Sample-level paleomagnetic and rock magnetic data can be obtained from the corresponding author upon reasonable request.

Appendix A. Supplementary material

Supplementary data to this article can be found online at https://doi.org/10.1016/j.precamres.2022.106786.

References

Åhäll, K.-I., Connelly, J.N., 2008. Long-term convergence along SW Fennoscandia: 330 m.y. of Proterozoic crustal growth. Precambrian Res. 163, 402–421.
Andersen, T., Griffin, W.L., Jackson, S.E., Knudsen, T.-L., Pearson, N.J., 2004. Mid-Proterozoic magmatic arc evolution at the southwest margin of the Baltic Shield. Lithos 73, 289–318.
Andersen, T., 2005. Terrane analysis, regional nomenclature and crustal evolution in the Southwest Scandinavian Domain of the Fennoscandian Shield. Geol. fören. Stockh. förh. 127, 159–168.
Berthelsen, A., 1980. Towards a palinspastic tectonic analysis of the Baltic Shield, in Cogne, J., Slansky, M. (Eds.), Geology of Europe, from Precambrian to the post-Hercynian sedimentary basins. Mem. du B.R.G.M., pp. 5-21.
Bingen, B., Mansfeld, J., Sigmond, E.M.O., Stein, H.J., 2002. Baltica-Laurentia link during the Mesoproterozoic: 1.27 Ga development of continental basins in the Sveconorwegian Orogen, southern Norway. Can. J. Earth Sci. 39, 1425–1440.
Bingen, B., Skår, Ø., Marker, M., Sigmond, E.M.O., Nordgulen, Ø., Ragnhildstveit, J., Mansfeld, J., Tucker, R.D., Liégeois, J.-P., 2005. Timing of continental building in the Sveconorwegian orogen, SW Scandinavia. Nor. J. Geol. 85, 87–116.
Bingen, B., Davis, W.J., Hamilton, M.A., Engvik, A.K., Stein, H.J., Skår, Ø., Nordgulen, Ø., 2008a. Geochronology of high-grade metamorphism in the

Sveconorwegian belt, S. Norway: U-Pb, Th-Pb, and Re-Os data. Nor. J. Geol. 88, 13–42.
Bingen, B., Nordgulen, Ø., Viola, G., 2008b. A four-phase model for the Sveconorwegian orogeny, SW Scandinavia. Nor. J. Geol. 88, 43–72.
Bingen, B., Viola, G., 2018. The early-Sveconorwegian orogeny in southern Norway: Tectonic model involving delamination of the sub-continental lithospheric mantle. Precambrian Res. 313, 170–204.
Bingen, B., Viola, G., Möller, C., Vander Auwera, J., Laurent, A.T., Andersson, J., 2018. The Mesoproterozoic Sveconorwegian orogeny: orogen scale interpretation of metamorphic and magmatic patterns supports an ultra-hot collision model, EGU General Assembly 2018. EGU, Vienna, pp. EGU2018-17218.
Bingen, B., Viola, G., Möller, C., Vander Auwera, J., Laurent, A.T., Keewok, Y.i., 2021. The Sveconorwegian orogeny. Gondwana Res. 90, 273–313.
Blereau, E., Johnson, T.E., Clark, C., Taylor, R.J.M., Kinny, P.D., Hand, M., 2017. Reappraising the P-T evolution of the Rogaland-Vest Agder Sector, southwestern Norway. Front. 8, 1–14.
Brown, L.L., McEnroe, S.A., 2004. Paleomagnetism of the Egersund-Ogna Anorthosite, Rogaland, Norway, and the position of Fennoscandia in the Late Proterozoic. Geophys. J. Int. 158, 479–488.
Brown, L.L., McEnroe, S.A., 2012. Paleomagnetism and magnetic mineralogy of Grenville metamorphic and igneous rocks. Adirondack Highland, USA, Precambrian Res. 212–213, 57–74.
Brown, L.L., McEnroe, S.A., 2015. 916 Ma Pole for southwestern Baltica: paleomagnetism of the Bjerkreim-Sokndal layered intrusion, Rogaland Igneous Complex, southern Norway. Geophys. J. Int. 203, 567–587. https://doi.org/10.1093/gji/ggv299.
Bybee, G.M., Ashwal, L.D., Shirey, S.B., Horan, M., Mock, T., Andersen, T.B., 2014. Pyroxene megacrysts in Proterozoic anorthosites: Implications for tectonic setting, magma source, and magmatic processes at the Moho. Earth Planet. Sci. Lett. 389, 74–85.
Bylund, G., 1992. Palaeomagnetism, mafic dykes and the Protogine Zone, southern Sweden. Tectonophysics 201, 49–63.
Cawood, P.A., Pisarevsky, S.A., 2006. Was Baltica right-way-up or upside-down in the Neoproterozoic? J. Geol. Soc. London 163, 753–759.
Cawood, P.A., Strachan, R., Cutts, K., Kinny, P.D., Hand, M., Pisarevsky, S., 2010. Neoproterozoic orogeny along the margin of Rodinia: Valhalla orogen, North Atlantic. Geology 38, 99–102.
Cawood, P.A., Strachan, R.A., Pisarevsky, S.A., Gladkochub, D.P., Murphy, J.B., 2016. Linking collisional and accretionary orogens during Rodinia assembly and breakup: implications for models of supercontinent cycles. Earth Planet. Sci. Lett. 449, 118–126.
Coint, N., Slagstad, T., Roberts, N.M.W., Marker, M., Røhr, T., Sørensen, B.E., 2015. The Late Mesoproterozoic Sirdal Magmatic Belt, SW Norway: Relationships between magmatism and metamorphism and implications for Sveconorwegian orogenesis. Precambrian Res. 265, 57–77.
Condie, K., 2013. Preservation and Recycling of Crust during Accretionary and Collisional Phases of Proterozoic Orogens: A Bumpy Road from Nuna to Rodinia. Geosciences 3, 240.
Corfu, F., 2019. The Sognefjell volcanic-subvolcanic complex – A late Sveconorwegian arc imbricated in the central Norwegian Caledonides. Precambrian Res. 331, 105353.
Cosca, M.A., Mezger, K., Essene, E.J., 1998. The Baltica-Laurentia connection: Sveconorwegian (Grenvillian) metamorphism, cooling, and unroofing in the Bamble Sector. Nor. J. Geol. 06, 539–552.
Cosca, M.A., O'Nions, R.K., 1994. A re-examination of the influence of composition on argon retentivity in metamorphic calcic amphiboles. Chem. Geol. 112, 39–56.
Culshaw, N.G., Jamieson, R.A., Ketchum, J.W.F., Wieck, N., Corrigan, D., Reynolds, P.H., 1997. Transect across the northwestern Grenville orogen, Georgian Bay, Ontario: polystage convergence and extension in the lower orogenic crust. Tectonics 16, 966–982.
Day, R., Fuller, M., Schmidt, V.A., 1977. Hysteresis properties of titanomagnetites: grain size and compositional dependence. Phys. Earth Planet. Inter. 13, 260–267.
de Haas, G.-J.-L.-M., Andersen, T., Vestin, J., 1999. Detrital zircon geochronology: New evidence for an old model for accretion of the southwest Baltic Shield. J. Geol. 107, 569–586.
de Haas, G.J.L.M., Nijland, T.G., Andersen, T., Corfu, F., 2002. New constraints on the timing of deposition and metamorphism in the Bamble sector, south Norway: zircon and titanite U-Pb data from the Nelaug area. GFF 124, 73–78.
Dominguez, A.R., Van der Voo, R., Torsvik, T.H., Hendricks,B.H.W., Abrajevitch, A., Domeir, M., Larsen, B.T., Rousse, S., 2011. The 270 Ma paleolatitude of Baltica and its significance for Pangea models Geophysical Journal International, 186 2011), pp. 529-550.
Elming, S.Å., Pisarevsky, S.A., Layer, P., Bylund, G., 2014. A palaeomagnetic and 40Ar/39Ar study of mafic dykes in southern Sweden: A new Early Neoproterozoic keypole for the Baltic Shield and implications for Sveconorwegian and Grenville loops. Precambrian Res. 244, 192–206.
Engvik and Austrheim, 2010. Formation of sapphirine and corundum in scapolitised and Mg-metasomatised gabbro. Terra Nova 22 (2010), 166–171.
Engvik, A.K., Mezger, K., Wortelkamp, S., Bast, R., Corfu, F., Korneliussen, A., Ihlen, P. M., Bingen, B., Austrheim, H., 2011. Metasomatism of gabbro – mineral replacement and element mobilization during the Sveconorwegian metamorphic event. J. Metamorph. Geol. 29, 399–423.
Engvik, A.K., Corfu, F., Solli, A., Austrheim, H., 2017. Sequence and timing of mineral replacement reactions during albitization in the high-grade Bamble lithotectonic domain. S-Norway. Precambrian Res. 291, 1–16.
Engvik, A.K., Taubald, H., Solli, A., Grenne, T., Austrheim, H., 2018. Dynamic metasomatism: stable isotopes, fluid evolution, and deformation of albite and scapolite metagabbro (Bamble lithotectonic domain, South Norway). Geofluids 2018, 22.
Enkin, R.J., 2003. The direction-correction tilt test: an all-purpose tilt/fold test for paleomagnetic studies. Earth Planet. Sci. Lett. 212, 151–166.
Evans, D.A.D., 2009. The paleomagnetically viable, long-lived and all-inclusive Rodinia supercontinent reconstruction in Murphy, J.B., Keppie, J.D., Hynes, A.J., eds., Ancient Orogens and Modern Analogues: Geol. Soc. London Spe. Pub., 327, 371-404.
Evans, D.A.D., Heaman, L.M., Trindade, R.I.F., D'Agrella-Filho, M.S., Smirnov, A.V., Catelani, E.L., 2010. Precise U-Pb baddeleyite ages from Neoproterozoic mafic dykes in Bahia, Brazil, and their paleomagnetic/paleogeographic implications. Proceedings, American Geophysical Union, Joint Assembly, Meeting of the Americas, Iguassu Falls, Brazil, Abstract GP31E–07.
Evans, D.A.D., 2013. Reconstructing pre-Pangean supercontinents Geol. Soc. Am. Bull. 125, 1735–1751.
Evans D.A.D., Trindade, R.I.F., Catelani, E.L., Agrella-Filho M.S.D., Heaman, L.M., Oliveira E.P., Söderlund, U., Ernst, R.E., Smirnov, A.V., Salminen, J.M., 2015. Return to Rodinia? Moderate to high palaeolatitude of the São Francisco/Congo craton at 920 Ma. Li, Z.-X., Supercontinent Cycles Through Earth History. Evans, D.A.D. & Murphy, J.B. (eds). Geol. Soc. Spec. Pub., London, 424.
Evans, D.A.D., Pesonen, L.J., Eglington, B.M., Elming, S.-Å., Gong, Z., Li, Z.-X., McCausland, P.J., Meert, J.G., Mertanen, S., Pisarevsky, S.A., Pivarunas, A.F., Salminen, J.M., Swanson-Hysell, N., Torsvik, T.H., Trindade, R.I.F., Veikkolainen, T., Zhang, S., 2021. Chapter 19. An expanding list of reliable paleomagnetic poles for Precambrian tectonic reconstructions. In: Pesonen, L.J., Salminen, J., Evans, D.A.D., Elming, S.-Å., Veikkolainen, T. (Eds.), Ancient Supercontinents and the Paleogeography of Earth. Elsevier, pp. 605–640. https://doi.org/10.1016/B978-0-12-818533-9.00007-2.
Fairchild, L.M., Swanson-Hysell, N.L., Ramezani, J., Sprain, C.J., and Bowring, S.A., 2017, The end of Mid-continent Rift magmatism and the paleogeography of Laurentia, Lithosphere, v. 9, p. 117–133, https:// DOI .org /10 .1130 /L580 .1.
Falkum, T., Petersen, J.S., 1980. The Sveconorwegian orogenic belt, a case of late-Proterozoic plate-collision. Geol. Rundsch. 69, 622–647.
Fisher, R.A., 1953. Dispersion on a sphere. Proc. Royal Soc. London, Series A 217, 295–305.
Gong, Z., Evans, D.A.D., Elming, S.-A., Söderlund, U., Salminen, J.M., 2018. Paleomagnetism, magnetic anisotropy, and U-Pb baddeleyite geochronology of the early Neoproterozoic Blekinge-Dalarna dolerite dykes. Sweden. Precambrian Res. 317, 14–32.
Gower, C., 1985. Correlations between the Grenville Province and Sveconorwegian orogenic belt - implications for Proterozoic evolution of the southern margin of the Canadian and Baltic Shields. In: Tobi, A.C., Touret, J.L.R. (Eds.), The Deep Proterozoic Crust in the North Atlantic Provinces. Reidel, Dordrecht, pp. 247–257.
Gower, C.F., Ryan, A.B., Rivers, T., 1990. Mid-Proterozoic Laurentia-Baltica: an overview of its geological evolution and a summary of the contributions made by this volume. In: Gower, C.F., Rivers, T., and Ryan, A.B. (Eds.), Mid-Proterozoic Laurentia-Baltica, Geol. Assoc. Canada, Spec. Pap. pp. 1-20.
Gower, C.F., Kamo, S.L., Kwok, K., Krogh, T.E., 2008. Proterozoic southward accretion and Grenvillian orogenesis in the interior Grenville Province in eastern Labrador: Evidence from U-Pb geochronological investigations. Precambrian Res. 165, 61–95.
Haggerty, S.E., 1991. Oxide textures - a mini-atlas. Rev. Mineral. 25, 129–219.
Halls, H.C., 1976. A Least-Squares Method to find a Remanence Direction from Converging Remagnetization Circles. Geophys. J. Int. 45 (2), 297–304. https://doi.org/10.1111/j.1365-246x.1976.tb00327.x.
Hanson, R.E., Rioux, M., Bowring, S., Gose, W.A., Bartholomew, T., Kilian, T.M., Evans, D.A.D., Panzik, J.E., Hoffmann, K.-H., Reid, A.B., 2011b. Constraints on Neoproterozoic intraplate magmatism in the Kalahari craton: Geochronology and paleomagnetism of ~890–795 Ma extension-related igneous rocks in SW Namibia and adjacent parts of South Africa: Geol. Soc. Am. Abs. with Prog. 43 (5), 371.
Harlov, D.E., 1992. Comparative oxygen barometry in granulites, Bamble Sector, S.E. Nor. J. Geol. 100, 447–464.
Harlov, D.E., 2000. b. Titaniferous magnetite ± ilmenite thermometry and titaniferous magnetite ± ilmenite ± orthopyroxene ± quartz oxygen barometry in granulite facies gneisses, Bamble sector, SE Norway: implications for the role of high-grade CO2-rich fluids during granulite genesis. Contrib. to Mineral. Petrol. 140, 180–197.
Hnat, J.S., van der Pluijm, B.A., Van der Voo, R., 2006, Primary curvature in the MidContinent Rift: Paleomagnetism of the Portage Lake Volcanics (northern Michigan, USA): Tectonophysics, v. 425, p. 71–82, HTTPS:// doi .org /10 .1016 j . tecto .2006 .07 .006.
Hoffmann, P.F., 1991. Did the breakout of Laurentia turn Gondwana inside-out? Science 252, 1409–1412.
Hynes, A., Rivers, T., 2010. Protracted continental collision—Evidence from the Grenville Orogen. Can. J. Earth Sci. 47 (5), 591–620.
Karlstrom, K.E., Åhäll, K.-I., Harlan, S.S., Williams, M.L., McLelland, J., Geissman, J.W., 2001. Long-lived (1.8-1.0 Ga) convergent orogen in southern Laurentia, its extensions to Australia and Baltica, and implications for refining Rodinia. Precambrian Res. 111, 5–30.
Kirschvink, J.L., 1980. The least-squares line and plane and the analysis of palaeomagnetic data. Geophys. J. Int. 62, 699–718.
Knudsen, T.L., Andersen, T., Whitehouse, M.J., Vestin, J., 1997. Detrital zircon ages from southern Norway – implications for the Proterozoic evolution of the southwestern Baltic shield. Contrib. to Mineral. Petrol. 130, 47–58.
Knudsen, T.-L., Andersen, T., 1999. Petrology and geochemistry of the Tromøy Gneiss Complex, south Norway, and alleged example of Proterozoic depleted lower continental crust. J. Petrol. 40, 909–933.

Kulakov, E.V., Smirnov, A.V., Diehl, J.F., 2013. Paleomagnetism of ~1.09 Ga Lake Shore Traps (Keweenaw Peninsula, Michigan): New results and implications, submitted to Can. J. Earth Sci. 50, V 11. https://doi.org/10.1139/cjes-2013-0003.
Laajoki, K., Corfu, F., Andersen, T., 2002. Lithostratigraphy and U-Pb geochronology of the Telemark supracrustals in the Bandak-Sauland area, Telemark, South Norway. Nor. J. Geol. 82, 119–138.
Li, Z.X., Bogdanova, S.V., Collins, A.S., et al., 2008. Assembly, configuration, and break-up history of Rodinia: A synthesis. Precambrian Res. 160, 179–210.
Lindsey, J.S., 1991. Self-Assembly in Synthetic Routes to Molecular Devices. Biological Principles and Chemical Perspectives: A Review. Cheminform, 22.
Maslov, A.V., 2004. Riphean and Vendian sedimentary sequences of the Timanides and Uralides, the eastern periphery of the East European Craton. Geol. Soc. Lond. Mem. 30, 19–35.
Maslov, A.V., Isherskaya, M.V., 2002. Riphean sedimentary sequences of the eastern and northeastern margins of the Eastern European craton. Russ. J. Earth Sci. 4, 271–276.
Maslov, A.V., Erdtmann, B.D., Ivanov, K.S., Ivanov, S.N., Krupenin, M.T., 1997. The main tectonic events, depositional history, and the paleogeography of the southern Urals during the Riphean-early Palaeozoic. Tectonophysics 276, 313–335.
McFadden, P.L., Jones, D.L., 1981. The fold test in paleomagnetism. Geophys. J. Roy. Astron. Soc. 135, 53–58.
McFadden, P.L., McElhinny, M., 1990. Classification of the reversal test in paleomagnetism. Geophys. J. Int. 103, 725–729.
McLelland, J.M., Selleck, B.W., Bickford, M.E., 2013. Tectonic Evolution of the Adirondack Mountains and Grenville Orogen Inliers within the USA. Geosci. Can. 40 (4), 318–352. https://doi.org/10.12789/geocanj.2013.40.022.
Meert, J.G., 2014a. Ediacaran-Early Ordovician paleomagnetism of Baltica: A review. Gondwana Res. 25, 159–169. https://doi.org/10.1016/j.gr.2013.02.003.
Meert, J.G., 2014b. Strange attractors, spiritual interlopers and lonely wanderers: The search for pre-Pangean supercontinents. Geosci. Front. 5, 155–166. https://doi.org/10.1016/j.gsf.2013.12.001.
Meert, J.G., Pivarunas, A.F., Evans, D.A.D., Pisarevsky, S.A., Pesonen, L.J., Li, Z.-X., Elming, S.-Å., Miller, S.R., Zhang, S., Salminen, J.M., 2020a. The magnificent seven: A proposal for modest revision of the Van der Voo (1990) quality index. Tectonophysics 790, 228549.
Mertanen, S., Pesonen, L.J., Huhma, H., 1996. Palaeomagnetism and Sm-Nd ages of the Neoproterozoic diabase dykes in Laanila and Kautokeino, northern Fennoscandia. Geol. Soc. Spec. Pub. London 112 (1), 331–358. https://doi.org/10.1144/GSL.SP.1996.112.01.18.
Nikishin, A.M., Ziegler, P.A., Stephenson, R.A., Cloetingh, S.A.P.L., Furne, A.V., Fokin, P.A., Ershov, A.V., Bolotov, S.N., Korotaev, M.V., Alekseev, A.S., Gorbachev, V.I., Shipilov, E.V., Lankreijer, A., Bembinova, E.Y., Shalimov, I.V., 1996. Late Precambrian to the Triassic history of the East European Craton: dynamics of sedimentary basin evolution. Tectonophysics 268, 23–63.
Nijland, T.G., Harlov, D.E., Andersen, T., 2014. The Bamble Sector, South Norway: A review. Geosci. Front. 5, 635–658.
Petersson, A., Scherstén, A., Bingen, B., Gerdes, A., J. Whitehouse, M., 2015b. Mesoproterozoic continental growth: U–Pb–Hf–O zircon record in the Idefjorden Terrane, Sveconorwegian Orogen. Precambrian Res. 261, 75-95.
Piispa, E.J., Smirnov, A.V., Pesonen, L.J., Roger H. Mitchell, R.H., 2018. Paleomagnetism and Geochemistry of ~1144-Ma Lamprophyre Dikes, Northwestern Ontario: Implications for the North American Polar Wander and Plate Velocities. J. Geophys. Res., 123, 6195-6214.
Piper, J.D.A., 2009. Uplift and cooling magnetization record in the Bamble and Telemark terranes, Sveconorwegian orogenic belt, SE Norway, and the Grenville-Sveconorwegian loop. Tectonophysics 463, 185–207.
Pisarevsky, S.A., Bylund, G., 2006. Palaeomagnetism of 935 Ma mafic dykes in southern Sweden and implications for the Sveconorwegian Loop. Geophys. J. Int. 166 (3), 1095–1104.
Pisarevsky, S.A., Wingate, M.T.D., Powell, C.M., Johnson, S., Evans, D.A.D., 2003. Models of Rodinia assembly and fragmentation. In: Yoshida, M., Windley, B.F., Dasgupta, S. (Eds.), Proterozoic East Gondwana: Supercontinent Assembly and Breakup. Geol. Soc. Spec. Pub. London, 206, 35–55.
Poorter, R.P.E., 1975. Paleomagnetism of Precambrian rocks of southeast Norway and south Sweden. Phys. Earth Planet. Inter. 10, 74–87.
Puchkov, V.N., 2010. Geology of the Urals and Cis-Urals. Actual Problems of Stratigraphy, Tectonics, Geodynamics and Metallogeny. Disain Poligraf Servis, Ufa (in Russian).
Puchkov, V.N., Bogdanova, S.V., Ernst, R.E., Kozlov, V.I., Krasnobaev, A.A., Söderlund, U., Wingate, M.T.D., Postnikov, A.V., Sergeeva, N.D., 2013. The ca. 1380 Ma Mashak igneous event of the Southern Urals. Lithos 174, 109–124.
Pullaiah, G., Irving, E., Buchan, K., Dunlop, D., 1975. Magnetization changes caused by burial and uplift, Earth and Planet. Sci. Lett. 28, 133–143.
Renne, P.R., Mundil, R., Greg Balco, G., Min, K., Ludwig, K.R., 2010. Joint determination of 40K decay constants and $^{40}Ar/^{40}K$ for the Fish Canyon sanidine standard, and improved accuracy for $^{40}Ar/^{39}Ar$ geochronology. Geochim. Cosmochim. Acta 74, 5349–5367.
Rivers, T., 2012. Upper-crustal orogenic lid and mid-crustal core complexes: signature of a collapsed orogenic plateau in the hinterland of the Grenville Province. Can. J. Earth Sci. 49, 1–42.
Rivers, T., Schwerdtner, W.M., 2015. Post-peak evolution of the Muskoka Domain, western Grenville Province: ductile detachment zone in a crustal-scale metamorphic core complex. Geosci. Canada 42, 403–436.
Roberts, A.P., Pike, C.R., Verosub, K.L., 2000. First-order reversal curve (FORC) diagrams: A new tool for characterizing the magnetic properties of natural samples. J. Geophys. Res. 105, 28.
Roberts, A.P., Heslop, D., Zhao, X., Pike, C.R., 2014. Understanding fine magnetic particle systems through the use of first-order reversal curve (FORC) diagrams. Rev. Geophys. 52, 557–602. https://doi.org/10.1002/2014RG000462.
Roberts, N.M.W., Slagstad, T., 2015. Continental growth and reworking on the edge of the Columbia and Rodinia supercontinents; 1.86–0.9 Ga accretionary orogeny in southwest Fennoscandia. International Geol. Rev. 57, 1582–1606.
Salminen, J., Pesonen, L.J., Mertanen, S., Vuollo, J., Airo, M.-L., 2009. Palaeomagnetism of the Salla Diabase Dyke, northeastern Finland, and its implication for the Baltica-Laurentia entity during the Mesoproterozoic. Palaeoproterozoic supercontinents and global evolution. Geol. Soc. Spec. Pub. London 323, 199–217.
Siedlecka, A., Roberts, D., Nystuen, J.P., Olovyanishnikov, V.G., 2004. Northeastern and northwestern margins of Baltica in Neoproterozoic time: evidence from the Timanian and Caledonian Orogens. In: Gee, D.G., Pease, V.L. (Eds.), The Neoproterozoic Timanide Orogen of Eastern Baltica, 30. Geol. Soc., Lon. Mem., pp. 169–190.
Slagstad, T., Roberts, N.M.W., Marker, M., Røhr, T.S., Schiellerup, H., 2013. A non-collisional, accretionary Sveconorwegian orogen. Terra Nova 25, 30–37.
Slagstad, T., Roberts, N.M.W., Kulakov, E., 2017. Linking orogenesis across a supercontinent; the Grenvillian and Sveconorwegian margins on Rodinia. Gondwana Res. 44, 109–115.
Slagstad, T., Roberts, N.M.W., Coint, N., Høy, I., Sauer, S., Kirkland, C.L., Marker, M., Røhr, T.S., Henderson, I.H.C., Stormoen, M.A., Skår, Ø., Sørensen, B.E., Bybee, G.M., 2018b. Magma-driven, high-grade metamorphism in the Sveconorwegian Province, SW Norway during the terminal stages of Fennoscandian Shield evolution. Geosphere 14, 861–882.
Slagstad, T., Kulakov, E., Kirkland, C.L., Roberts, N.M.W., Ganerød, M., 2019. Breaking the Grenville-Sveconorwegian link in Rodinia reconstructions. Terra Nova 31, 430–437.
Slagstad, T., Marker, M., Roberts, N.M.W., Saalmann, K, Kirkland, C., L., Evgeniy Kulakov, E., V., Ganerød, M., Røhr, T.,S., Møkkelgjerd, S.,H.,H., Granseth, A., Sørensen, B., E., 2020. The Sveconorwegian orogeny – Reamalgamation of the fragmented southwestern margin of Fennoscandia. Precambrian Res., 350. DOI: 10.1016/j.precamres.2020.105877.
Stearn, J.E.F., Piper, J.D.A., 1984. Paleomagnetism of the Sveconorwegian mobile belt of the Fennoscandian Shield. Precambrian Res. 23, 201–246.
Torsvik, T.H., 2003. The Rodinia Jigsaw Puzzle. Science 300, 1379–1381.
Torsvik, T.H., Eide, E.A., Meert, J.G., Smethurst, M.A., Walderhaug, H.J., 1998. The Oslo Rift: New palaeomagnetic and 40Ar/39Ar age constraints. Geophys. J. Int. 135, 1045–1059.
Walderhaug, H.J., Torsvik, T.H., Eide, E.A., Sundvoll, B., Bingen, B., 1999. Geochronology and paleomagnetism of the Hunnedalen dykes, SW Norway: Implications for the Sveconorwegian apparent polar wander loop. Earth Planet. Sci. Lett. 169 (1), 71–83.
Warnock, A.C., Kodama, K.P., Zeitler, P.K., 2000. Using thermochronometry and low-temperature demagnetization to accurately date Precambrian paleomagnetic poles. J. Geophys. Res. 105, 19435–19453.
Watson, G.S., Enkin, R.J., 1993. The fold test in paleomagnetism as a parameter estimation problem. Geophys. Res. Lett. 20, 2135–2137.
Weil, A.B., Van der Voo, R., Mac Niocaill, C., Meert, J.G., 1998. The Proterozoic supercontinent Rodinia: Paleomagnetically derived reconstruction for 1100 to 800 Ma Earth Planet. Sci. Lett. 154, 13–24.
Wilson, R.L., Watkins, N.D., 1967. Correlation of magnetic polarity and petrological properties in Columbia Plateau Basalts. Geophys. J. Roy. Astron. Soc. 12, 405–429.

Further reading

Torsvik, T.H., Van der Voo, R., Preeden, R., Mac Niocaill, C., Steinberger, B., Doubrovine, P.V., Van Hinsbergen, D.J.J., Domeier, M., Gaina, C., Tohver, E., 2012. Phanerozoic polar wander, paleogeography and dynamics, Earth Sci. Rev. 114, 325–368.